AD-A089 608 AEROSPACE CORP EL SEGUNDO CA CHEMISTRY AND PHYSICS LAB F/G 21/9.1
EXPECTED DETECTION LIMITS OF HYDRAZINE-BASED ROCKET FUELS AND T--ETC(U)
AUG 80 G L LOPER, A R CALLOWAY, M A STAMPS F04701-79-C-0080
UNCLASSIFIED TR-0080(5970-09)-1 SD-TR-80-55 NL

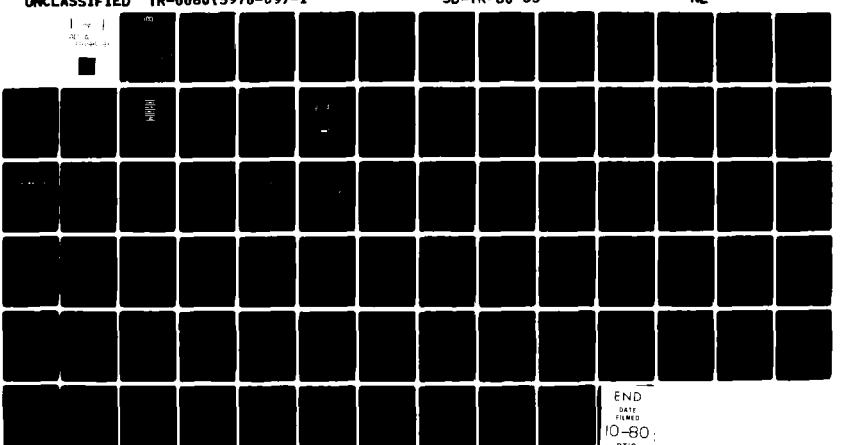

END
DATE FILMED
10-80
DTIC

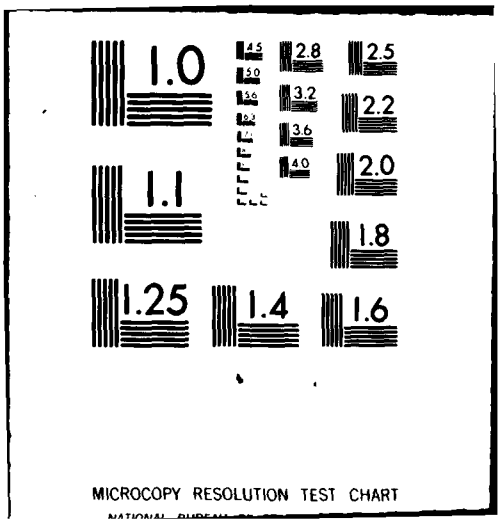
1.0
1.1
1.25
1.4
1.6
1.8
2.0
2.2
2.5
2.8
3.2
3.6
4.0
4.5
5.0
5.6
6.3
MICROCOPY RESOLUTION TEST CHART

Expected Detection Limits of Hydrazine-Based Rocket Fuels and Their Selected Oxidation Products by $^{12}C^{16}O_2$ Laser Spectroscopic Techniques

G. L. LOPER, A. R. CALLOWAY, M. A. STAMPS, and J. A. GELBWACHS
Chemistry and Physics Laboratory
Laboratory Operations
The Aerospace Corporation
El Segundo, Calif. 90245

15 August 1980

Interim Report

THE AEROSPACE CORPORATION

Prepared for

SPACE DIVISION
AIR FORCE SYSTEMS COMMAND
Los Angeles Air Force Station
P.O. Box 92960, Worldway Postal Center
Los Angeles, Calif. 90009

This interim report was submitted by The Aerospace Corporation, El Segundo, CA 90245, under Contract No. F04701-79-C-0080 with the Space Division, Contracts Management Office, P.O. Box 92960, Worldway Postal Center, Los Angeles, CA 90009. It was reviewed and approved for The Aerospace Corporation by Seymour Siegel, Director, Chemistry and Physics Laboratory. Gerhard E. Aichinger was the project officer for Mission-Oriented Investigation and Experimentation (MOIE) Programs.

This report has been reviewed by the Public Affairs Office (PAS) and is releasable to the National Technical Information Service (NTIS). At NTIS, it will be available to the general public, including foreign nations.

This technical report has been reviewed and is approved for publication. Publication of this report does not constitute Air Force approval of the report's findings or conclusions. It is published only for the exchange and stimulation of ideas.

Gerhard E. Aichinger
Project Officer

FOR THE COMMANDER

EVAN R. EROSSMAN
Chief, Contracts Management Office

UNCLASSIFIED

SECURITY CLASSIFICATION OF THIS PAGE (When Data Entered)

(19) REPORT DOCUMENTATION PAGE	READ INSTRUCTIONS BEFORE COMPLETING FORM
(18) 1. REPORT NUMBER SD-TR-80-55 ✓	2. GOVT ACCESSION NO. AD-A089 608
(6) 4. TITLE (and Subtitle) Expected Detection Limits of Hydrazine-Based Rocket Fuels and Their Selected Oxidation Products by $^{12}C^{16}O_2$ Laser Spectroscopic Techniques	(9) 5. TYPE OF REPORT & PERIOD COVERED Interim technical rept.s
	(14) 6. PERFORMING ORG. REPORT NUMBER TR-0080(5970-09)-1 ✓
(10) 7. AUTHOR(s) G. L. Loper, A. R. Calloway, M. A. Stamps, J. A. Gelbwachs	(15) 8. CONTRACT OR GRANT NUMBER(s) F04701-79-C-0080
9. PERFORMING ORGANIZATION NAME AND ADDRESS The Aerospace Corporation ✓ El Segundo, California 90245	10. PROGRAM ELEMENT, PROJECT, TASK AREA & WORK UNIT NUMBERS (12) 782
11. CONTROLLING OFFICE NAME AND ADDRESS Space Division Air Force Systems Command Los Angeles, California 90009	(11) 12. REPORT DATE 15 August 1980 ✓
	13. NUMBER OF PAGES 73
14. MONITORING AGENCY NAME & ADDRESS (if different from Controlling Office)	15. SECURITY CLASS. (of this report) Unclassified
	15a. DECLASSIFICATION/DOWNGRADING SCHEDULE

16. DISTRIBUTION STATEMENT (of this Report)

Approved for public release; distribution unlimited.

17. DISTRIBUTION STATEMENT (of the abstract entered in Block 20, if different from Report)

18. SUPPLEMENTARY NOTES

19. KEY WORDS (Continue on reverse side if necessary and identify by block number)

hydrazine fuel detection, toxic vapor analysis, trace molecule detection, ambient air monitoring, analytical spectroscopy, carbon dioxide laser spectroscopy, photoacoustic technique, optoacoustic technique

20. ABSTRACT (Continue on reverse side if necessary and identify by block number)

This report details the progress of the effort toward the development of CO_2 laser spectroscopic techniques for the detection of trace airborne levels of toxic hydrazine-based rocket fuels and some of their potentially toxic air oxidation products. The health hazards to humans resulting from exposure to these compounds, even at very low concentrations, are of increasingly great concern. The Air Force needs improved detection techniques that will permit

DD FORM (FACSIMILE) 1473

UNCLASSIFIED 409383

SECURITY CLASSIFICATION OF THIS PAGE (When Data Entered)

these compounds to be monitored on a real-time basis down to the 30 part-per-billion (ppb) level in the ambient air near hydrazine-fuel production and storage facilities and at missile launch sites.

Three CO_2 laser spectroscopic techniques are considered for monitoring airborne levels of hydrazine fuels and their selected degradation products. These are the $^{12}C^{16}O_2$ laser-based photoacoustic, conventional long-path absorption, and lidar (laser radar) detection techniques. As part of the information needed to estimate the detection sensitivites of the hydrazine fuels by each technique, $^{12}C^{16}O_2$ laser vapor phase absorption cross sections were measured at about 77 $^{12}C^{16}O_2$ laser wavelengths and are reported for the rocket fuels hydrazine, monomethylhydrazine (MMH), and unsymmetrical dimethylhydrazine (UDMH), as well as for their selected air oxidation products, dimethylamine, trimethylamine, and methanol. Similar data are presented from the literature for the hydrazine-fuel degradation products ammonia and methylamine. From these data, it is estimated that detection sensitivites of 30 ppb should be obtainable for each of the hydrazine fuels in the presence of typical ambient air concentrations of water vapor by the $^{12}C^{16}O_2$ laser photoacoustic technique. Under similar conditions, practical detection sensitivities for hydrazine, MMH, and UDMH of about 70, 140, and 130 ppb, respectively, should be possible using a long-path (100-m) absorption cell, while lidar detection sensitivites of about 50, 90, and 60 ppb, respectively, would be expected using a range cell path length of 100 meters.

Analysis of the $^{12}C^{16}O_2$ laser absorption spectra of the aforementioned air oxidation products of the hydrazines indicates that, at their anticipated airborne concentrations, these compounds will not interfere with hydrazine detection. Consideration of the concentrations of pollutants typically found in urban air and their infrared spectral properties indicates that the estimated $^{12}C^{16}O_2$ laser detection limits of the hydrazines should not be significantly increased by the presence of typical air pollutants.

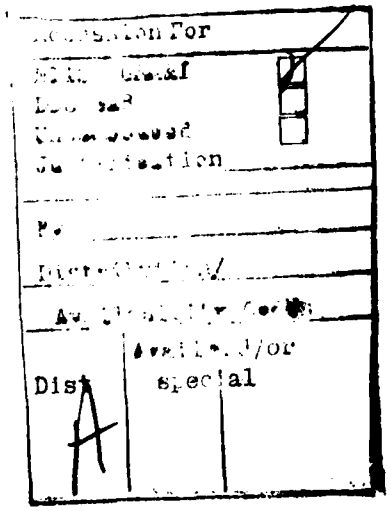

CONTENTS

FIGURES

TABLES

I. INTRODUCTION

In this report, an account is presented of the investigation of the use of carbon dioxide (CO_2) laser spectroscopic techniques for real-time monitoring of toxic vapors at the parts per billion (ppb) level in the work environment important to the Air Force and its contractors. This work in the current program is aimed at detecting the rocket fuels hydrazine, monomethylhydrazine (MMH), and unsymmetrical dimethylhydrazine (UDMH), and some of the potentially toxic air oxidation products of MMH and UDMH. If these compounds can be successfully monitored at part-per-billion levels by CO_2 laser spectroscopic techniques, it is anticipated that many other airborne toxic substances of concern to the Air Force will be detectable at similar low levels by the same techniques.

We are investigating CO_2 laser-based photoacoustic, conventional long-path absorption, and laser radar (lidar) spectroscopic techniques as methods of monitoring the levels of toxic vapors in the ambient air. Each of these techniques is based on the detection of selective absorption by the molecule of interest of infrared radiation from a wavelength-tunable CO_2 laser.

The excitation wavelengths selected for the detection of a particular molecule depend upon the wavelengths of its absorbances as well as those of potentially interfering species. The wavelength region between ~8.5 and 12.5 μm is most suitable for ambient air detection of trace molecules because of the lack of absorption in this spectral region by most of the major atmospheric gases. Absorption by atmospheric water vapor and CO_2 severely limits detection sensitivities at other infrared wavelengths. Therefore, we chose the well-developed, reliable CO_2 laser as the excitation source for a possible detector of toxic vapors in the ambient air. The $^{12}C^{16}O_2$ laser can produce over 100 discrete wavelengths between ~9.1 and 11.0 μm[1] where a large number of molecules (including the hydrazine-based rocket fuels and their toxic air oxidation products of current concern) exhibit strong,

highly characteristic absorption bands. Other isotopic CO_2 species can extend the laser spectral output to almost 12 μm.[1]

To determine the feasibility of using CO_2 laser-based detection techniques to monitor the levels of toxic vapors in the ambient air, it is necessary to measure high-resolution absorption cross sections for these compounds as a function of CO_2 laser excitation wavelength. These data are needed to determine whether the toxic vapors of concern exhibit CO_2 laser high-resolution absorption spectra that can be specifically detected in the presence of expected interferences. These data are also required to permit accurate estimation of the detection sensitivities of these compounds by each of the CO_2 laser spectroscopic techniques under investigation. In this report are discussed vapor phase absorption spectra taken with a $^{12}C^{16}O_2$ laser for the rocket fuels hydrazine, MMH, and UDMH, and for the selected hydrazine fuel air oxidation products ammonia,* methylamine,* dimethylamine, trimethylamine, and methanol. These oxidation products are among those that may interfere with detection of the hydrazines. In addition, the detection of dimethylamine and trimethylamine is of interest, because these compounds may undergo further atmospheric reactions to form potentially carcinogenic compounds.[2] High-resolution CO_2 laser spectra of the MMH and/or UDMH air oxidation products formaldehyde monomethylhydrazone, formaldehyde dimethylhydrazone, and N-nitrosodimethylamine will be determined in the future and reported in a separate document.

In Section II, the Air Force's need to develop improved techniques to monitor airborne levels of the hydrazines and some of their degradation products is described. The CO_2 laser-based spectroscopic techniques under investigation for the real-time monitoring of these toxic vapors in the current program are also described in Section II. In Section III, the experimental apparatus and procedures used to determine the CO_2 laser

*Literature data are reported here for ammonia and methylamine.

high-resolution absorption spectra of the toxic vapors of concern are described. The CO_2 laser spectra determined to date for these compounds are presented in Section IV. Based on these high resolution spectra, a discussion of the expected CO_2 laser detectabilities of each of these compounds when photoacoustic, conventional long-path absorption, and lidar spectroscopic detection techniques are employed is presented in Section V. Conclusions are outlined in Section VI.

II. BACKGROUND

A. TOXIC VAPORS OF CURRENT SD CONCERN

A sensitive, selective, and reliable instrument for real-time detection of a wide variety of toxic vapors is being developed in response to the desire of the Air Force's Space Division (SD) to better protect the health of its own and its contractors' personnel. Such an instrument will also help SD and its contractors meet increasingly strict Occupational Safety and Health Administration (OSHA) and Environmental Protection Agency (EPA) requirements on the use of controlled toxic substances. The associated requirements to demonstrate that the workplace levels of toxic vapors are less than certain standard amounts will require much improved analytical techniques for the detection of these compounds.

EPA and OSHA restrictions on the use of toxic substances can have a significant impact on Air Force operations. This was demonstrated several years ago as the continuing availability of the rocket fuel UDMH became of great concern to the Air Force when its sole supplier almost had to terminate production because of difficulties in meeting OSHA standards on allowable worker exposure to a carcinogenic reaction intermediate, N-nitrosodimethylamine (NDMA), then used in the UDMH synthesis.[3] This particular problem should be alleviated by synthesis procedures that do not employ NDMA. However, the Air Force is also concerned about operations involving the use of the rocket fuels hydrazine, MMH, and UDMH because of possible adverse health effects of these compounds and some of their atmospheric degradation products.

During routine handling as fuels, the volatile hydrazines could be inadvertently released into the ambient air as a result of spillage, purging of transfer lines, or clean-up procedures. These compounds are highly toxic, and have been found in recent animal experiments to exhibit carcinogenic and mutagenic activity.[4,5] As a result, both the American

Conference of Governmental Industrial Hygienists (ACGIH) and the National Institute of Occupational Safety and Health (NIOSH) recently listed these compounds among industrial substances suspected of having carcinogenic potential toward humans. In 1977, ACGIH adopted time-weighted average threshold limit values over an 8-hour workday for exposure to airborne levels of hydrazine, MMH, and UDMH of 100, 200, and 500 ppb, respectively.[6] More recently, NIOSH suggested to the Department of Labor that even stricter standards for the hydrazines should be established. NIOSH recommended occupational exposure ceilings for hydrazine, MMH, and UDMH of 30, 40, and 60 ppb, respectively, over a 2-hour period. OSHA is expected to adopt one of these sets of threshold values as its new standards for the hydrazines. The proposed new standards allow up to 30 times less than current standards.

The analytical methods currently used to detect the hydrazines near production and storage facilities or near missile launch sites are neither sensitive nor specific enough for monitoring on a real-time basis at the expected new threshold levels. The analytical techniques now used to monitor the hydrazines in air give values averaged over the sampling period. With sufficient sampling times, the NIOSH-recommended gas chromatographic technique is sensitive to the hydrazines down to the new NIOSH-proposed levels.[7] Continuous monitors, however, are needed to measure peak levels of the hydrazines. Development of real-time monitors for the hydrazines based on chemiluminescence[8] and electrochemistry[9] is beginning. A near real-time instrument, using a moving paper tape impreganted with a color test reagent, has just become available commercially.[10] It is anticipated that the chemiluminescence, electrochemical, and paper tape monitors, in their present form, will not provide sufficient specificity to adequately distinguish one hydrazine from another, or the hydrazines from some of their atmospheric degradation products such as the hydrazones. The CO_2 laser-based detection methods should be more suitable for monitoring a wide range of compounds than are the chemiluminescence, electrochemical, and paper tape monitors.

In addition to concern about the adverse health effects of the hydrazines, there is a growing concern that some of the atmospheric degradation products of the hydrazines may be even more hazardous than the parent compounds. For example, it has been found that N-nitrosodimethylamine (NDMA), the same compound previously used in UDMH synthesis and one of the most potent carcinogens known, is formed in small amounts as a result of air oxidation reactions of UDMH.[11] Dimethylamine (DMA) and trimethylamine (TMA), other products formed in air oxidation reactions of UDMH,[11] can form NDMA as the result of reactions in typical NO_x polluted urban atmospheres.[2] The health hazards of the major UDMH air oxidation product, formaldehyde dimethylhydrazone (FDH),[12] and the major MMH air oxidation product, formaldehyde monomethylhydrazone (FMH), are not known. However, based on the similarity of the chemical structures of FDH [$(CH_3)_2N\text{-}N{=}CH_2$] and FMH [$^{CH_3}_{H}{>}N\text{-}N{=}CH_2$] to the corresponding parent hydrazines [$(CH_3)_2N\text{-}NH_2$ or $^{CH_3}_{H}{>}N\text{-}NH_2$] and to NDMA [$(CH_3)_2N\text{-}N{=}O$], the compounds FDH and FMH might be expected to exhibit toxic or carcinogenic properties similar to those of the hydrazines or NDMA.

Although adequate analytical procedures are available for the sensitive and selective monitoring of NDMA in the ambient air[13,14] none has been established for other potentially hazardous atmospheric degradation products of the hydrazines such as FDH and FMH. As more thorough investigations of the atmospheric degradation reactions of the hydrazines are carried out, more compounds may be identified as deleterious to human health, and methods for their detection will be needed. A single analytical instrument is needed that is capable of rapidly and specifically monitoring airborne levels in the ppb region of not only hydrazine, MMH, and UDMH, but also of their selected atmospheric degradation products such as NDMA, DMA, TMA, FDH, and FMH. Such an instrument will be even more necessary as the number of EPA and OSHA controlled toxic substances increases and their threshold limit levels are lowered. The CO_2 laser spectroscopic techniques for monitoring airborne toxic substances may fulfill this important need.

B. CO_2 LASER SPECTROSCOPIC TECHNIQUES UNDER INVESTIGATION

Molecules that undergo a dipole moment change with a change in geometry exhibit absorption bands in the infrared region of the electromagnetic spectrum.[15] When a molecule absorbs infrared radiation, it is excited to a higher vibrational or vibrational-rotational energy state. The positions and intensities of these bands depend on the size, type of bonding, and geometry of the molecule. As a result, a molecule's infrared spectral characteristics can provide a "fingerprint" that uniquely identifies it.[16]

To provide the selectivity required for trace detection of toxic vapors in the ambient air, multicomponent analysis is necessary. Particular species must be identified in the presence of others. Infrared laser spectroscopy can further enhance the high detection specificity obtainable with an infrared spectrophotometer equipped with an incoherent excitation source; a laser excitation source can provide an excitation bandwidth at least 100 times narrower than can be achieved with a typical infrared spectrometer equipped with an incoherent excitation source. The narrower bandwidth output of a laser source can resolve the underlying fine rotational structure in an infrared absorption band more readily than can a conventional spectrophotometer. This can be visualized by considering two hypothetical molecules A and B that absorb in the same general wavelength region. The absorption band contours of A and B are shown under conditions of large and narrow bandwidth excitation in Figs. 1a and 1b, respectively. Under conditions of large bandwidth excitation, as with a conventional spectrophotometer, the underlying fine rotational structure of the two absorption profiles remains unresolved, and the two molecules are not easily distinguished. However, upon excitation with a laser source (in this case, a laser source with a large number of discrete tunable lines) one component can be identified in the presence of another, or several others, if these molecules exhibit distinct high-resolution spectral features. Laser infrared spectroscopy thus greatly increases the possibility of

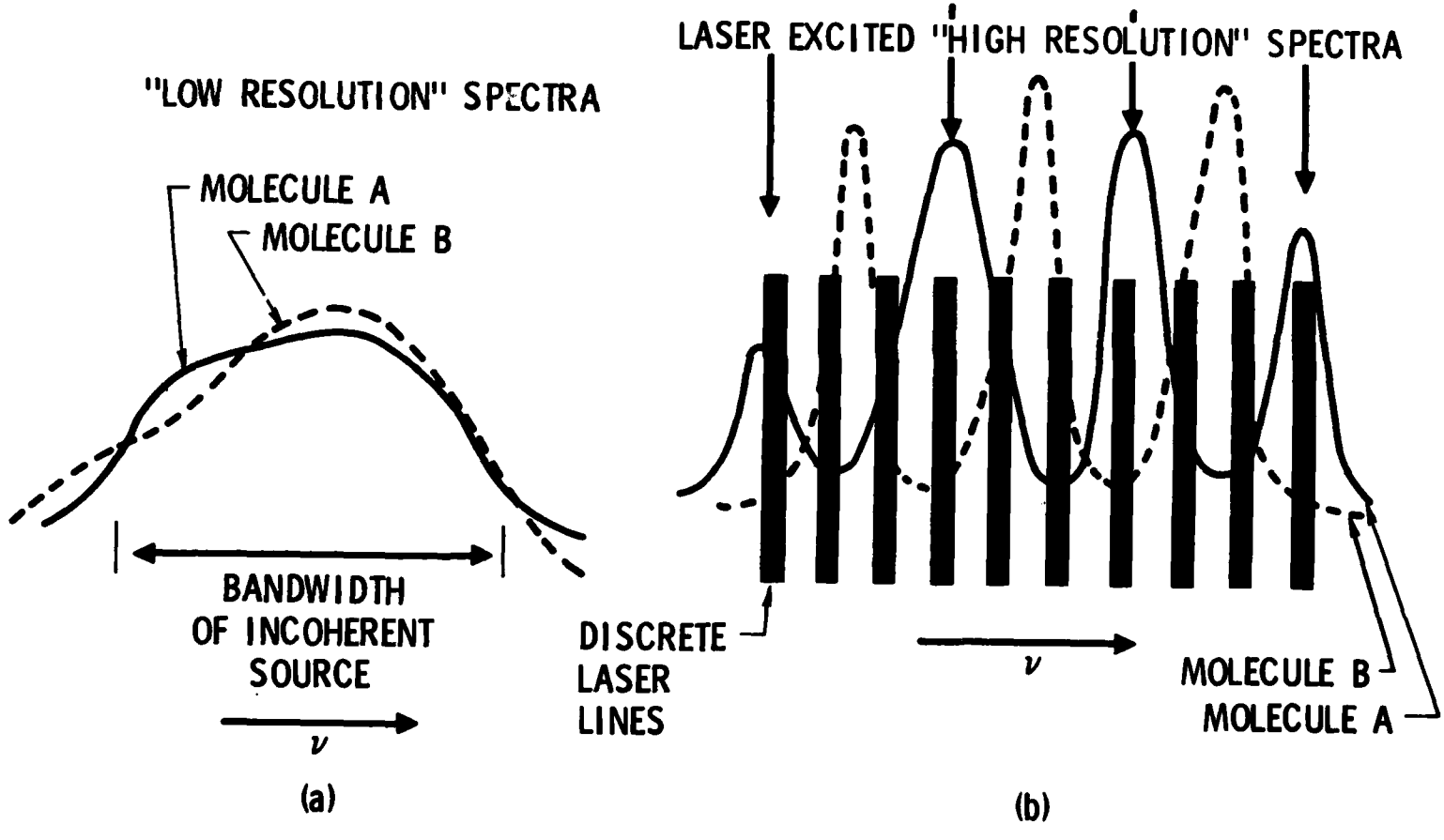

Fig. 1. Low vs High-Resolution Spectra for Hypothetical Molecules A and B

multicomponent analysis and discrimination from interferences compared with conventional infrared spectroscopy.

It is evident from Fig. 1b that, over a given wavelength region, the specificity of laser spectroscopic detection techniques will increase with the increasing density of available laser excitation wavelengths.* Because of the large number of closely spaced tunable wavelengths available from the R and P branches of its 9.4- and 10.4-μm bands (see Fig. 2),[17] the CO_2 laser is particularly well-suited for the highly specific excitation of the large number of molecules that absorb in the 9 to 11-μm wavelength region.

Infrared laser long-path absorption, lidar, and photoacoustic techniques can also provide highly sensitive detection of molecules.[18] By long-path absorption techniques, molecules that absorb at a particular laser wavelength are detected by monitoring the decrease in the laser light intensity as it passes through the air sample being analyzed. Long-path absorption measurements are conventionally made as shown in Fig. 3 with a sample cell of limited dimensions by the use of mirrors to obtain multiple passes of the monochromatic laser beam through the air sample.

Remote ambient measurements can be made by lidar techniques. By lidar methods, a laser beam propagates into the atmosphere to a remote region and interacts with the species being measured. The scattered radiation then returns to a receiver, most often colocated with the laser transmitter. The scattered light is then converted into electrical signals that, when processed, yield information about the concentration and distance of the species of interest.

The infrared laser photoacoustic technique, illustrated in Fig. 4, involves an intensity-modulated laser beam used to selectively vibrationally

*This is valid up to the limit set by pressure broadening of molecular absorption lines at one atmosphere pressure. The broadened line width is about 7.5 GHz or 0.25 cm^{-1} under these conditions. Thus, detection specificities would increase with increasing density of lines up to a density of about four lines/cm^{-1}.

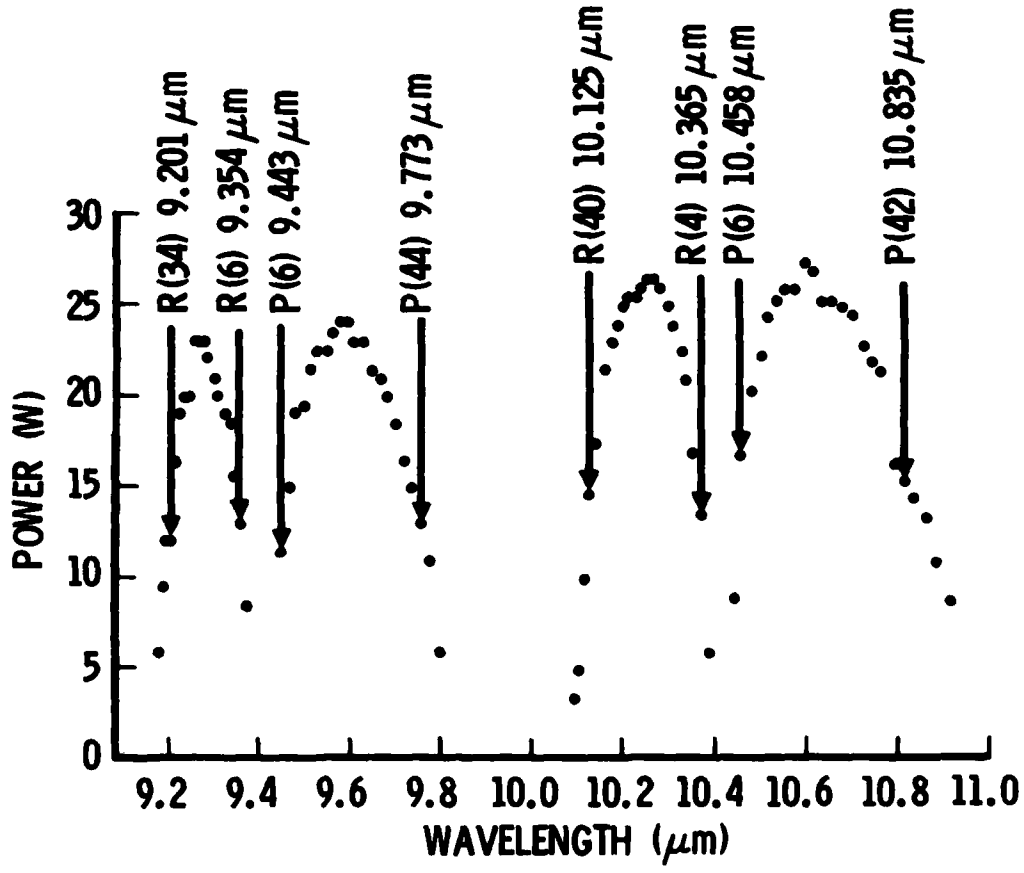

Fig. 2. Plot of Radiant Flux vs Wavelength of a Typical $^{12}C^{16}O_2$ Infrared Laser

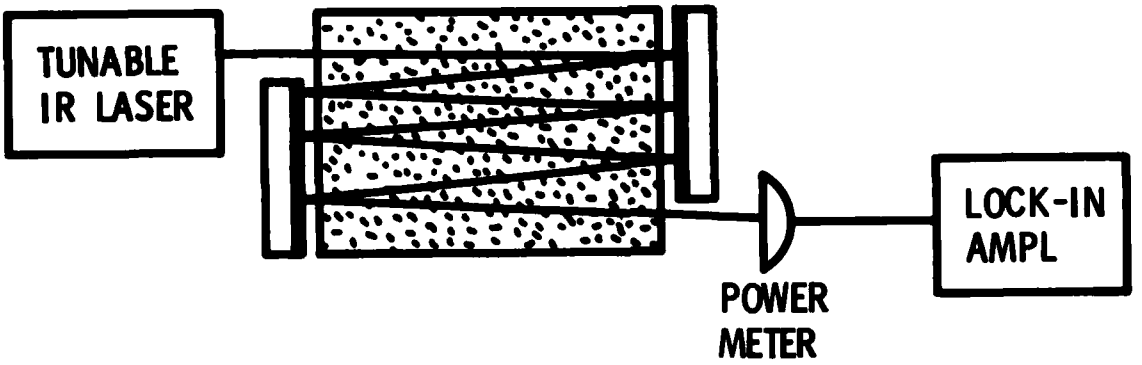

Fig. 3. Long-Path Infrared Absorption

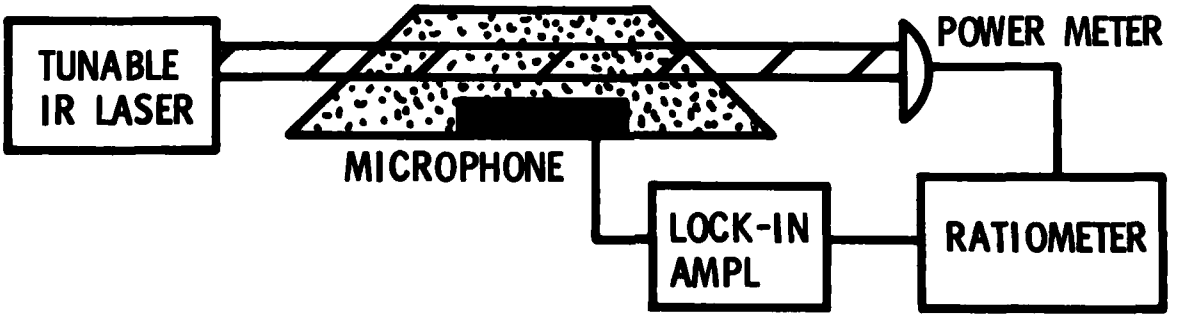

Fig. 4. Laser Photoacoustic Detection

excite the molecules of interest in a small-diameter closed cell. The energy periodically absorbed by these molecules is transferred through collisions with the surrounding nonabsorbing host gas molecules (N_2 and O_2) into periodic increases in the temperature of the entire gas mixture. This produces a periodic pressure pulse in the closed cell, which can be sensitively detected by a pressure transducer or, if the laser intensity is modulated at frequencies in the audio region, by a microphone.

Photoacoustic detection is expected to be more sensitive than long-path absorption and lidar techniques.[19] In any absorption measurement, the sensitivity is ultimately limited by the difficulty of measuring the small difference in the large intensities of the incident and transmitted light beams; photoacoustic detection, however, measures a small absorption signal against a null background.

The interference-free detection capabilities of each of the foregoing $^{12}C^{16}O_2$ laser-based techniques for the molecules studied here are estimated in Section V. These estimates are derived from the molecules' high-resolution absorption cross sections and from assumption of state-of-the-art detection sensitivities for each technique. In Section III, the experimental procedures and equipment used to determine the high-resolution absorption cross sections of these molecules are described.

III. EXPERIMENTAL

Two different CO_2 laser systems were used to measure the high-resolution vapor phase absorption cross sections of the hydrazines and some of their air oxidation products as a function of CO_2 laser wavelength.

Early measurements were made with a Sylvania Model 950A CO_2 laser that was line-tunable only within the 10.4-μm ($00^\circ 1$-$10^\circ 0$) $^{12}C^{16}O_2$ band. The output obtainable from this laser was normally limited to 26 wavelengths of the 10.4-μm $^{12}C^{16}O_2$ band [R32(10.171 μm) to R8(10.333 μm) and P8(10.476 μm) to P32(10.719 μm)]. The Sylvania laser used a sealed-off laser tube. The laser tube had zinc selenide Brewster windows which provided a vertically polarized output. Wavelength selection was performed by a totally reflecting, 80 groove/mm original aluminum grating placed in the rear reflecting position of the laser cavity. The output coupler was a 3-m radius-of-curvature, 70% reflecting mirror. The output mirror and the grating were separated from the laser tube by a low-expansion, hermetically sealed quartz cavity. This quartz cavity was water cooled to achieve the thermal stability required for long operation at a single wavelength with minimal amplitude variation. The optical cavity length of the laser was 77 cm. The grating was mounted on a piezoelectric transducer capable of varying the laser cavity length to permit the cavity mode to be tuned to the center of the selected laser transition. The laser control unit consisted of a regulated dc power supply for the laser tube and a highly stable dc supply for the piezoelectric transducer. The laser had an output power of almost 3 W in a TEM_{00} mode for its strongest laser lines. The manufacturer specifications on the laser amplitude stability were 5% long term and 0.5% short term.

Because the commercial (Sylvania) CO_2 laser used for these early measurements was tunable over only 26 lines of its 10.4-μm band, a $^{12}C^{16}O_2$ laser that was tunable over both its 9.4-μm ($00^\circ 1$-$02^\circ 0$) and 10.4-μm ($00^\circ 1$-$10^\circ 0$) bands was assembled from components available at The Aerospace Corporation.

This laser, which was used for most of the measurements reported here, was tunable over 36 wavelengths in the 9.4-μm $^{12}C^{16}O_2$ band [R36(9.192 μm) to R6(9.355 μm) and P6(9.443 μm) to P44(9.774 μm)], and over 41 wavelengths in the 10.4-μm $^{12}C^{16}O_2$ band [R40(10.124 μm) to R4(10.365 μm) and P4(10.441 μm) to P46(10.884 μm)]. The laser was operated in continuous-flow mode using a vacuum pump and a cylinder of the laser gas mixture 13.5% nitrogen, 4.5% carbon dioxide, and 82.0% helium supplied by Air Products, Inc. Laser tube gas pressures between 10 and 15 Torr were used. The Aerospace-fabricated laser tube was 127-cm long and fitted with zinc selenide Brewster windows. Wavelength selection was obtained with a PTR Optics 135 groove/mm, 2.54-cm diameter, gold-coated, 95% efficient grating. The grating was held in an Aerospace-fabricated, water-cooled copper block. Efficient cooling of the grating was essential for high-amplitude stability of the laser. A 2.54-cm-diameter, 10-m radius-of-curvature, zinc selenide output coupler (II-VI, Inc.) was used. This output coupler, which was 83% reflective, was mounted in Burleigh PZ-90 piezoelectric aligner/translator to permit the laser cavity to be tuned. The laser optical cavity length was 163 cm. A 20-kV, current-regulated dc power supply, previously designed and fabricated at Aerospace, provided voltage to the laser tube. A Hewlett-Packard 6516A dc power supply provided voltage to the piezoelectric aligner/translator. The laser had a TEM_{oo} mode output power of greater than 5 W on its strongest lines.

The optical arrangement used for the high-resolution absorption cross-section measurements in the early portion of the study is presented in Fig. 5. It consisted of the Sylvania CO_2 laser, 30-cm path length sample, and reference gas cells equipped with zinc selenide Brewster windows, zinc selenide beam splitters, and polished copper mirrors. The beam splitters and mirrors were necessary to permit measurement of the relative transmittance of infrared radiation through the cells with a power meter (either Scientech, Model 36/0001 or Coherent Radiation, Model 201). A CO_2 laser spectrum analyzer (Optical Engineering, Model 16-A) was used

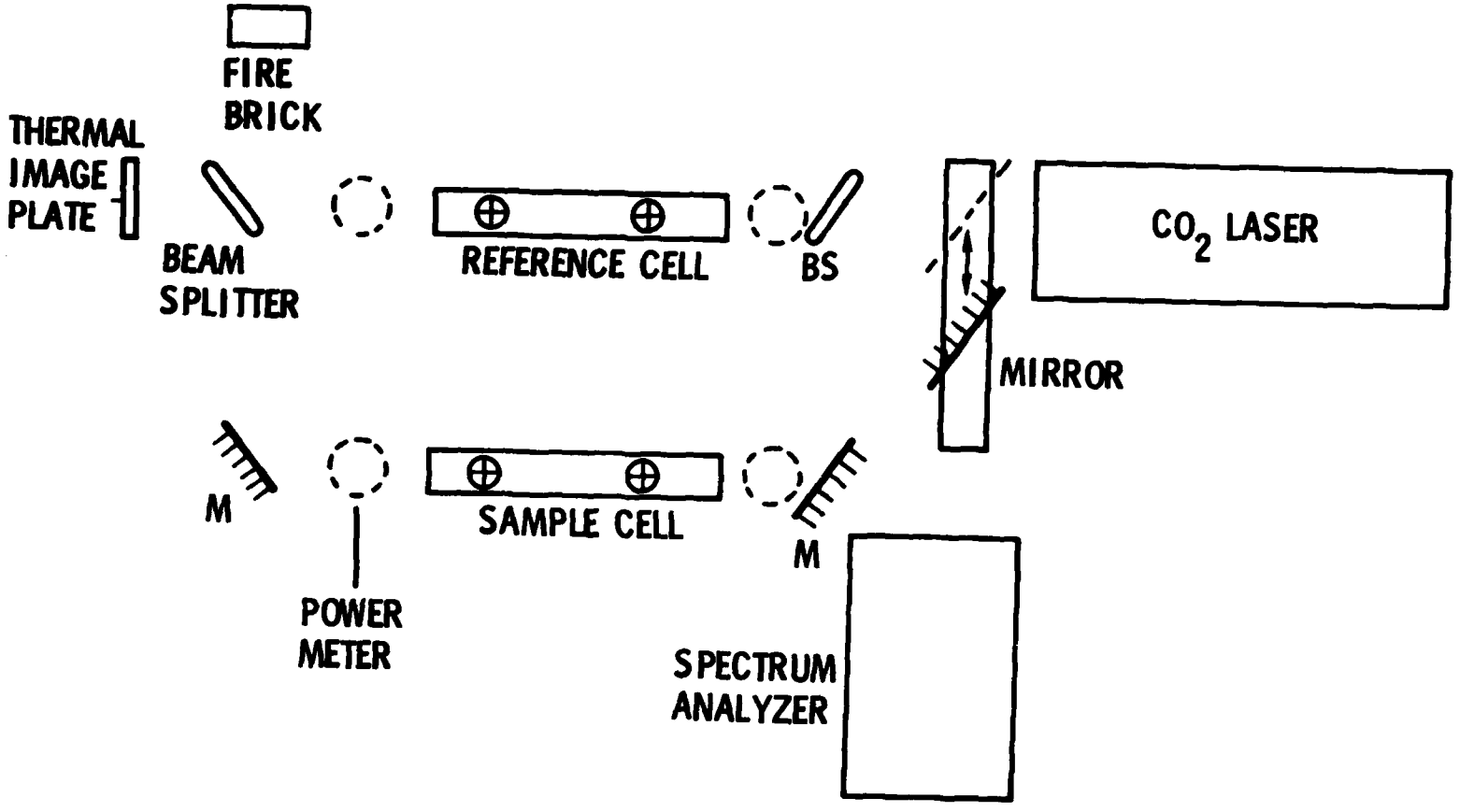

Fig. 5. Experimental Optical Arrangement for CO_2 Laser Spectrometer

to monitor the laser wavelength, and the shape of the beam mode pattern transmitted through the cell was monitored using thermal image plates. An optical arrangement similar to that in Fig. 5 was used for measurements with the Aerospace-assembled CO_2 laser, except that a separate reference cell was not used. Instead, reference-cell measurements were made on a sample cell filled with nitrogen only.

The high-resolution absorption cross sections $\sigma(\lambda)$, in units of $cm^{-1}atm^{-1}$, were determined as a function of CO_2 laser wavelength λ for hydrazine, MMH, UDMH, ammonia, dimethylamine, trimethylamine, and methanol by evaluating the relationship

$$\left[\frac{I(\lambda)_S}{I_o(\lambda)_S}\right]\left[\frac{I_o(\lambda)_R}{I(\lambda)_R}\right] = \exp\left[-\sigma(\lambda)\,p\,\ell\right] \qquad (1)$$

Here $I(\lambda)_S$ and $I_o(\lambda)_S$ represent the intensities of light transmitted through and incident on the sample cell, respectively, while $I(\lambda)_R$ and $I_o(\lambda)_R$ are comparable quantities for the reference cell. In this case, the sample cell was filled with known pressure p (in units of atmospheres) of one of the foregoing compounds and nitrogen was added to bring the total pressure in the cell to one atmosphere. The reference cell was filled with one atmosphere of nitrogen only. The quantity ℓ represents the sample cell path length in centimeters. The absorption measurements were made in an atmosphere of nitrogen to model the pressure broadening of the absorption lines of these compounds that would occur in the ambient air.

Throughout this study, three or more $I_o(\lambda)$ and $I(\lambda)$ measurements were generally made at each laser line for a given sample pressure. Higher pressures of the hydrazines were generally used for the absorption measurements made with the Aerospace-assembled laser than with the Sylvania laser. These higher hydrazine pressures resulted in more precise absorption measurements.

Our initial absorption measurements were taken with a 30-cm path length, 1.22-cm inside diameter, cylindrical glass sample cell. When this cell was used, the observed absorption for the hydrazines decreased slightly over the several hours measurements were performed. This decrease was attributed to surface-catalyzed degradation reactions and/or surface adsorption effects on the walls of the cell.* This problem was alleviated by the use of a sample cell for these measurements that had a surface-to-volume ratio of 0.28 cm^{-1}, about 12 times less than that of the cell initially used. The lower surface-to-volume ratio cell was fabricated by attaching 1.85-cm outside diameter glass tubing extensions to opposite sides of a 5-liter flask. This tubing was cut at Brewster's angle, and the zinc selenide windows were attached to the extensions with General Electric RTV-60 (a silicon rubber). The nearest edge of each Brewster window was 2 cm from the spherical bulb. The spherical glass sample cell was also equipped with an outer mixing loop to facilitate rapid and efficient gas mixing by convection.

The sources for the compounds studied are as follows: hydrazine (MCB anhydrous, 97% min), MMH (Aldrich, 98% min), UDMH (Aldrich, 95% min), ammonia (Matheson, anhydrous 99.99% min), dimethylamine (Matheson, 99.0% min), trimethylamine (Matheson, 99.0% min), and methanol (Mallinckrodt, anhydrous AR, 99.5% min). The high purities of these compounds were confirmed by comparing their low-resolution vapor-phase infrared spectra determined on a Perkin-Elmer 467 grating infrared spectrophotometer with standard spectra for these compounds given in the literature.[20-23] The $^{12}C^{16}O_2$ laser absorption spectra of each compound were found to also be consistent with their low-resolution standard spectra.

*Surface-catalyzed degradation reactions are not anticipated to be a significant problem in a real-field instrument. These instruments will probably be operated in a stopped-flow mode. The sample gas will have residence times of only a few minutes, since measurements will be performed only at several wavelengths with time scales of a few seconds per laser line.

Small quantities of these compounds were placed in evacuable storage tubes or bulbs where they were degassed at liquid nitrogen or dry ice temperatures on a mercury-free, greaseless vacuum line prior to use. The hydrazines, dimethylamine, and trimethylamine were pumped on at dry ice temperatures to facilitate removal of impurity ammonia. The pressures of these gases added to the absorption cell were determined by use of a Baratron pressure gauge (MKS Instruments, Inc.) with a 77 H-10 pressure head. Matheson Research purity nitrogen (99.9995% min.) was used as the buffer gas throughout the study. The pressures of nitrogen added were determined with a Matheson gauge (Model 63-5601).

IV. RESULTS

To be detectable by CO_2 laser spectroscopic techniques, a molecule's absorption bands must overlap one of the wavelength regions of CO_2 laser output. Figure 6 shows the vapor-phase transmission spectra of hydrazine, MMH, and UDMH in the 8- to 12-μm region as determined at a spectral resolution of ~2cm^{-1} with a Perkin Elmer 467 infrared spectrometer equipped with an incoherent source. The cross-hatched areas in Fig. 6 correspond to the wavelength regions of strong $^{12}C^{16}O_2$ laser output, i.e., the intervals of full-width-half-maximum output for the P and R branches of the 9.4- and 10.4-μm bands in Fig. 2.

The spectra of hydrazine and MMH exhibit absorbances that overlap the 10.4-μm $^{12}C^{16}O_2$ laser band; UDMH exhibits absorption in both the 9.4- and 10.4-μm bands. Similar spectra of ammonia, methylamine, dimethylamine, trimethylamine, methanol, formaldehyde monomethylhydrazone, formaldehyde dimethylhydrazone, and N-nitrosodimethylamine indicate that these hydrazine fuel degradation products also possess absorption bands that overlap portions of the $^{12}C^{16}O_2$ laser output.

Spectra obtained with a conventional infrared spectrophotometer can indicate which molecules are suitable for detection by CO_2 laser spectroscopic techniques. Such spectra, however, generally do not reveal underlying rotational fine structure in an infrared band. Therefore, absorption coefficients determined with a laser source may differ greatly from those measured with a broader band conventional spectrophotometer. Differences of up to an order of magnitude between absorption coefficients determined by a laser source and those determined by a spectrophotometer with an incoherent source may be possible, even when rotational fine structure remains unresolvable. High-resolution absolute absorption cross sections are thus needed as a function of CO_2 laser excitation wavelength for the determination of realistic detectabilities of molecules by CO_2 laser methods. The large differences possible between the absorption cross sections of molecules measured with the use of a laser source and with a broader band conventional

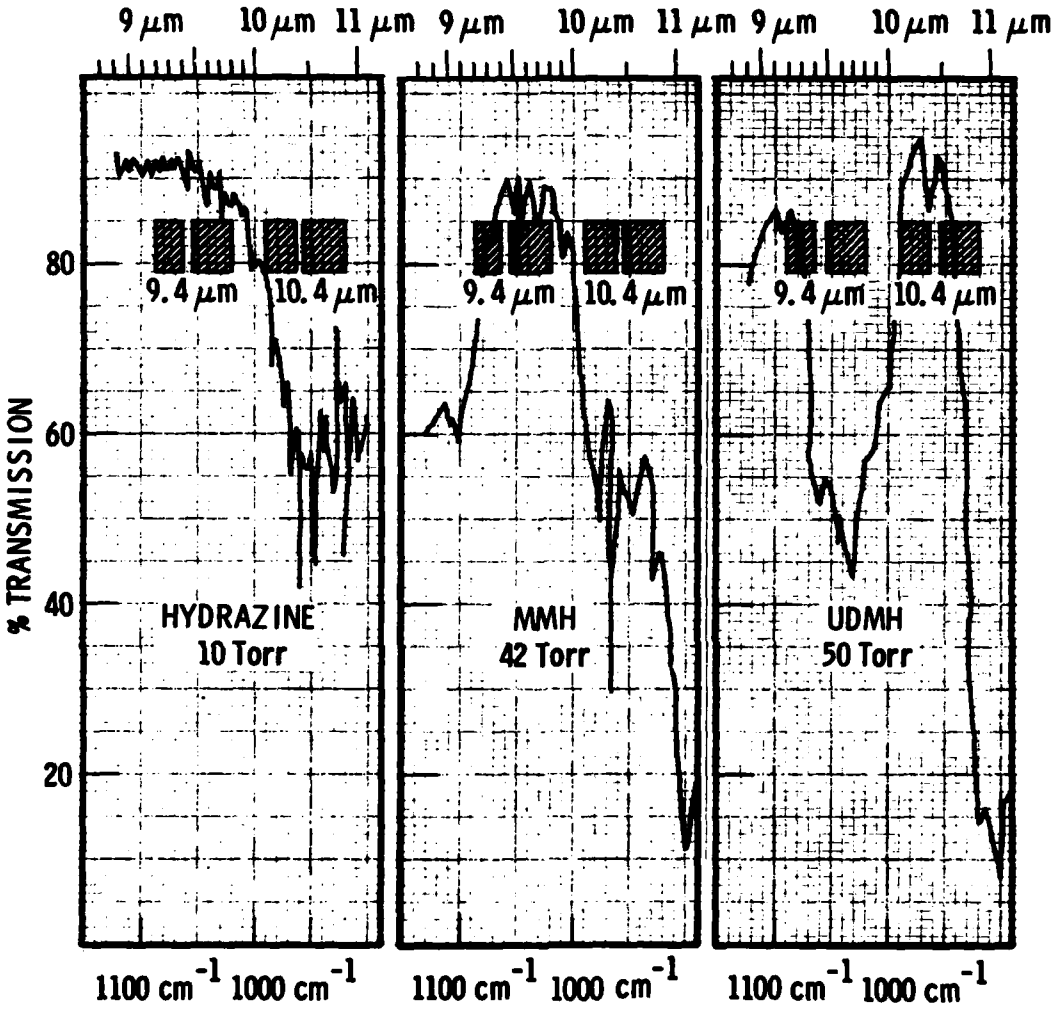

Fig. 6. Low-Resolution Infrared Hydrazine Spectra (Path length 8.7 cm)

spectrophotometer are illustrated in Fig. 7 for ammonia. In this figure, ammonia possesses resolvable rotational fine structure, and differences up to a factor of 25 are observed between cross sections determined with a CO_2 laser and those determined with a conventional infrared spectrophotometer. The higher peak absorptions obtained under conditions of narrowband excitation may permit enhanced detection sensitivities to be obtained. The increased detection specificities obtainable with a laser source are discussed in Section I.

The high-resolution vapor-phase CO_2 laser absorption spectra determined in this study for hydrazine, MMH, and UDMH are presented in Figs. 8 through 10. Similar spectra, either from the literature or determined here, for ammonia, methylamine, dimethylamine, trimethylamine, and methanol are presented in Figs. 11 through 15. The data given in Figs. 8 through 15 are also presented in Table I. The high-resolution absorption cross section data for each molecule were determined after the absorption cell was buffered to a total pressure of one atmosphere with pure nitrogen. Since collisional broadening effects by nitrogen and oxygen are of similar magnitude, these data should accurately represent the absorption cross sections that would be observed for these molecules in the ambient air. For the low pressures of the hydrazines or hydrazine fuel degradation products used in this study, self-broadening should not contribute significantly. The widths of the CO_2 laser lines used to determine the absorption cross sections in this study were on the order of 300 MHz or 0.01 cm^{-1}, while the bandwidths of atmospheric pressure-broadened molecular rotational lines are approximately 7.5 GHz or 0.25 cm^{-1}. Thus, the absorption cross sections at each laser line should be insensitive to slight frequency variations in the laser line positions that result from small fluctuations in the laser cavity length. All measurements presented here were made at room temperature, 295°K.

The spectral properties of the hydrazines and their possible air oxidation products are described below as separate groups.

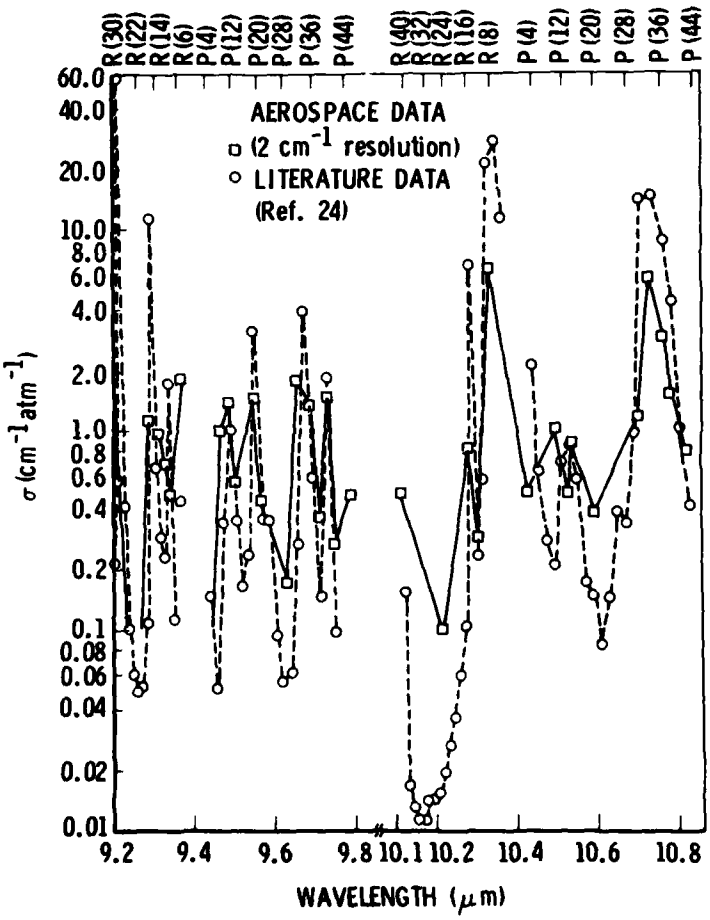

Fig. 7. Comparison of $^{12}C^{16}O_2$ Laser Absorption Spectrum vs 2 cm^{-1} Absorption Spectrum of Ammonia

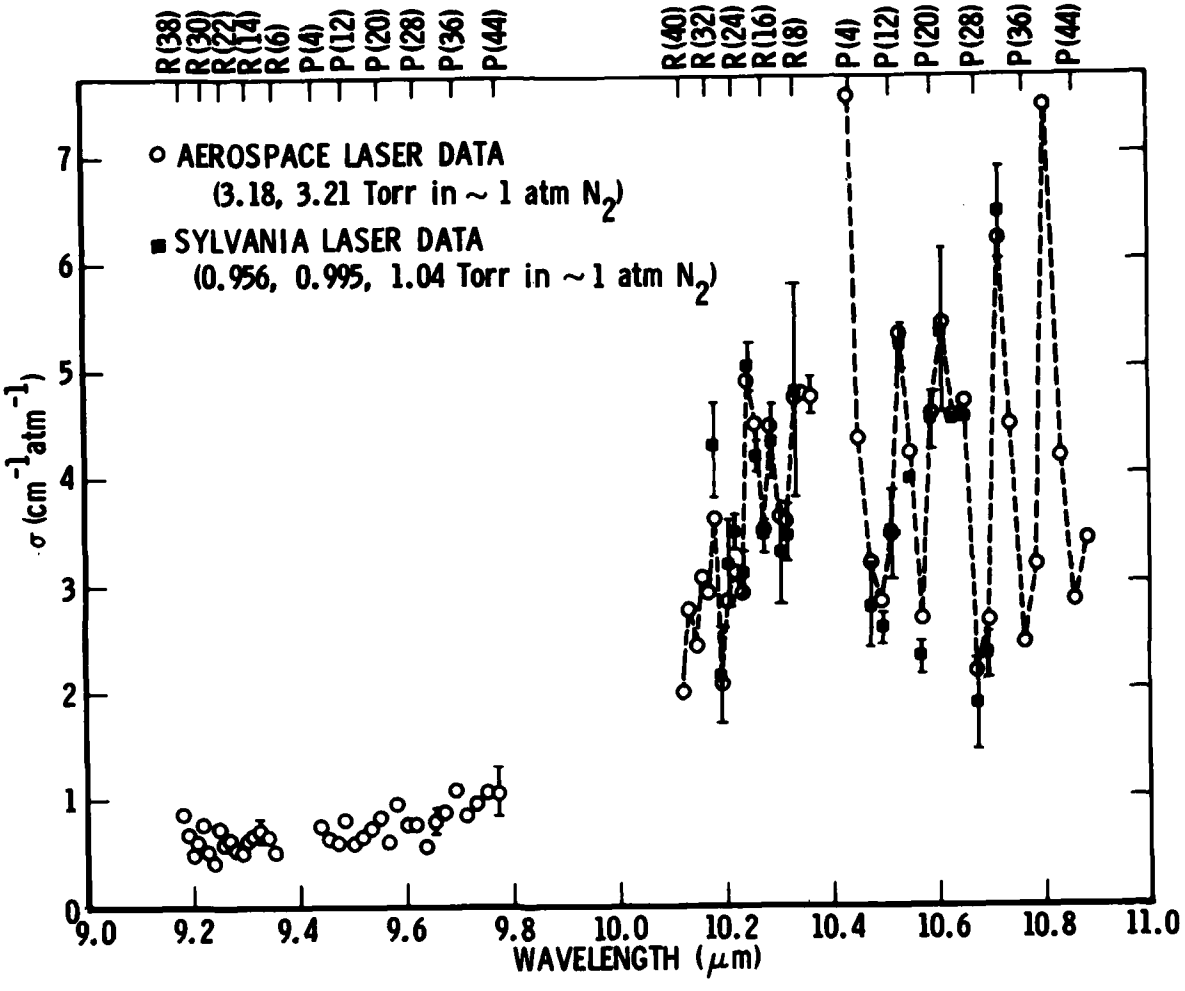

Fig. 8. $^{12}C^{16}O_2$ Laser Absorption Spectrum of Hydrazine

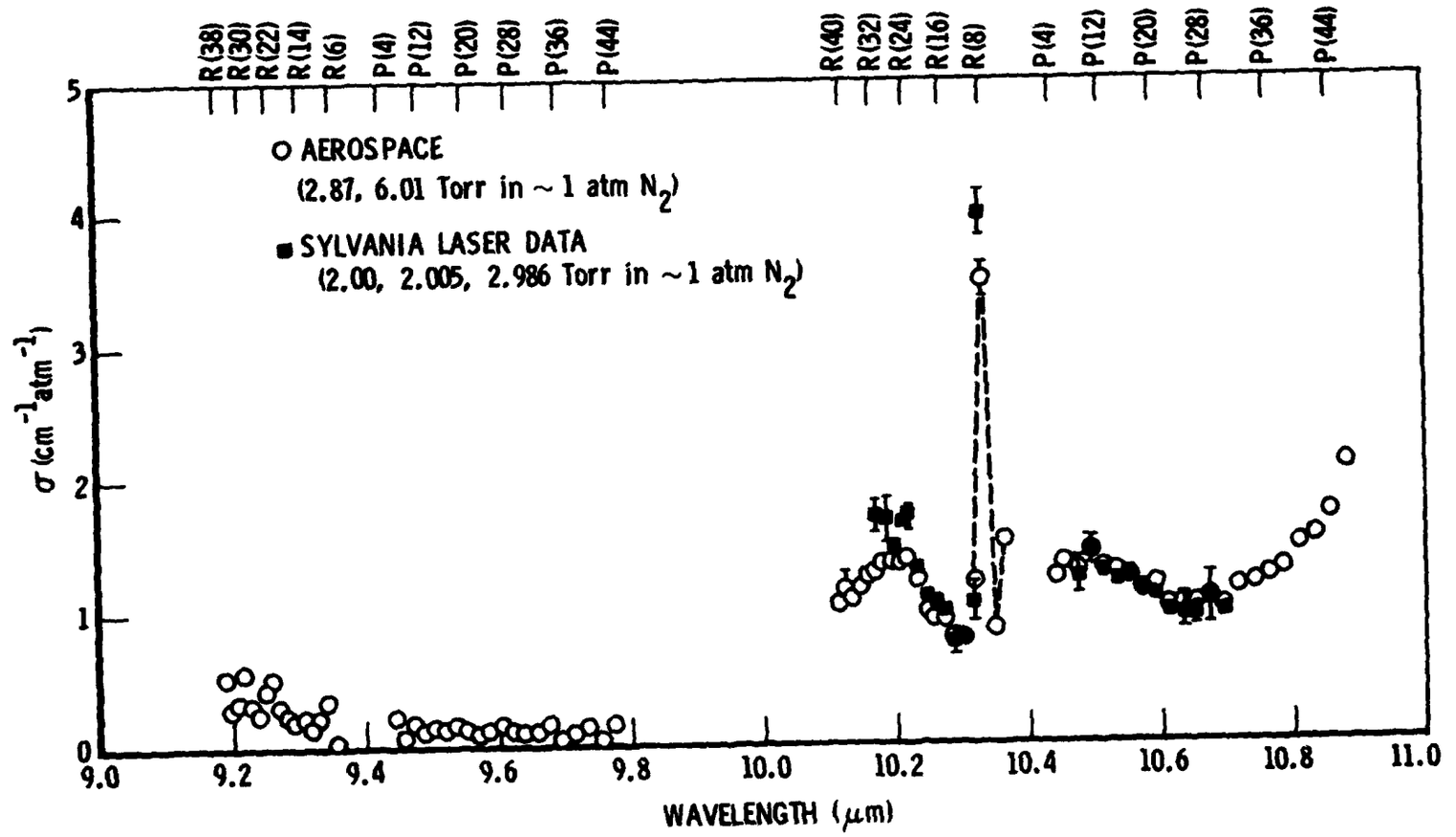

Fig. 9. $^{12}C^{16}O_2$ Laser Absorption Spectrum of MMH

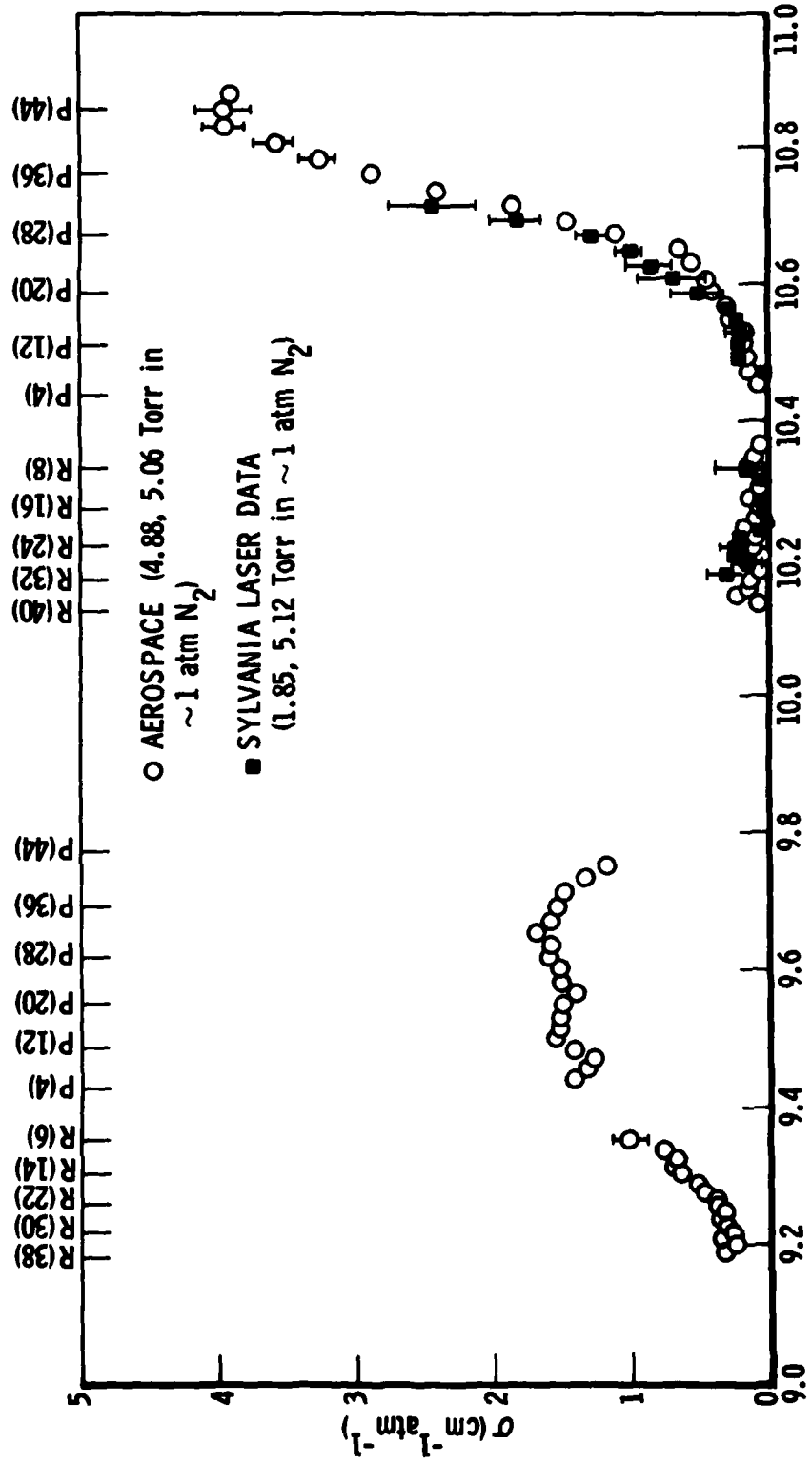

Fig. 10. $^{12}C^{16}O_2$ Laser Absorption Spectrum of UDMH

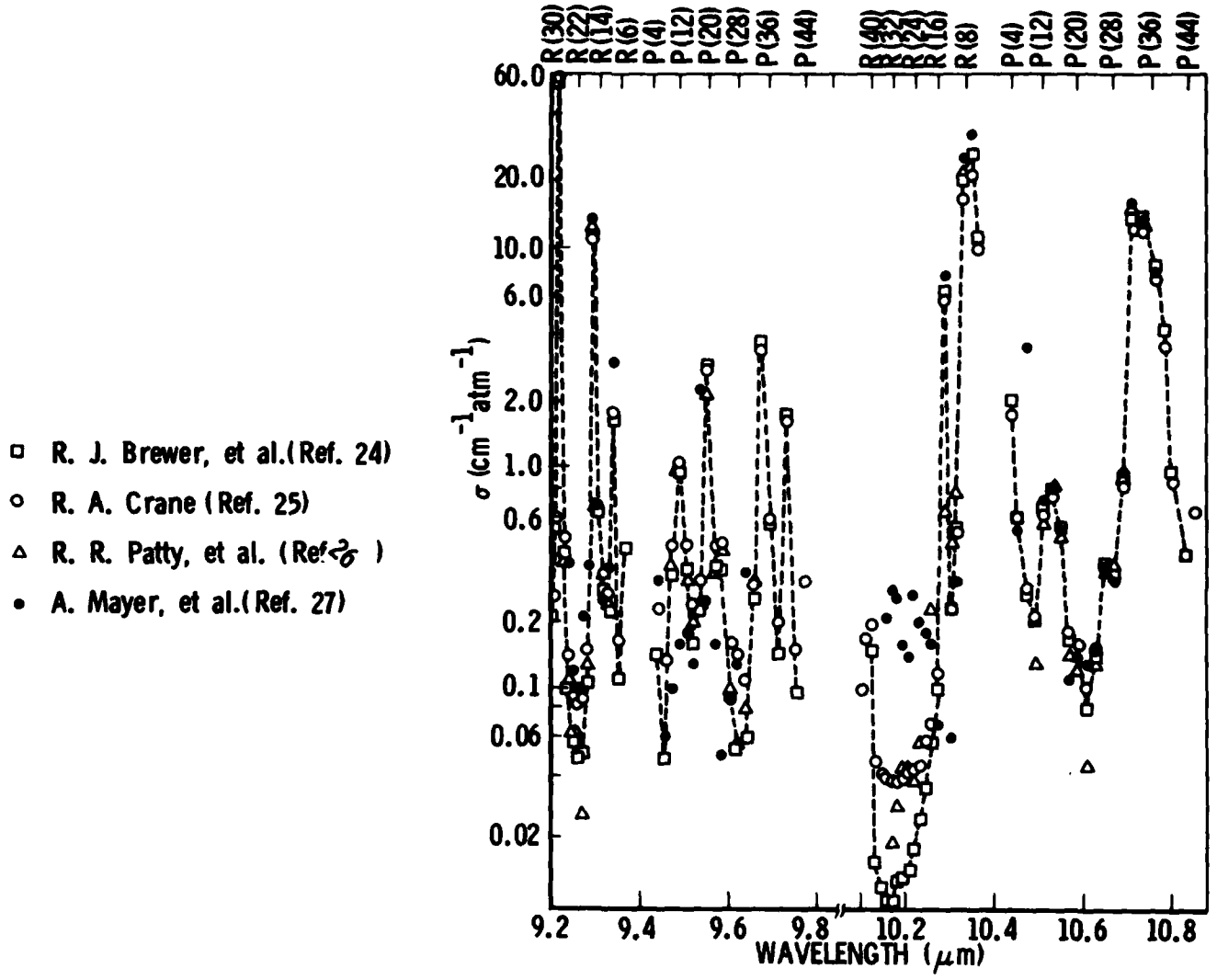

Fig. 11. $^{12}C^{16}O_2$ Laser Absorption Spectrum of Ammonia

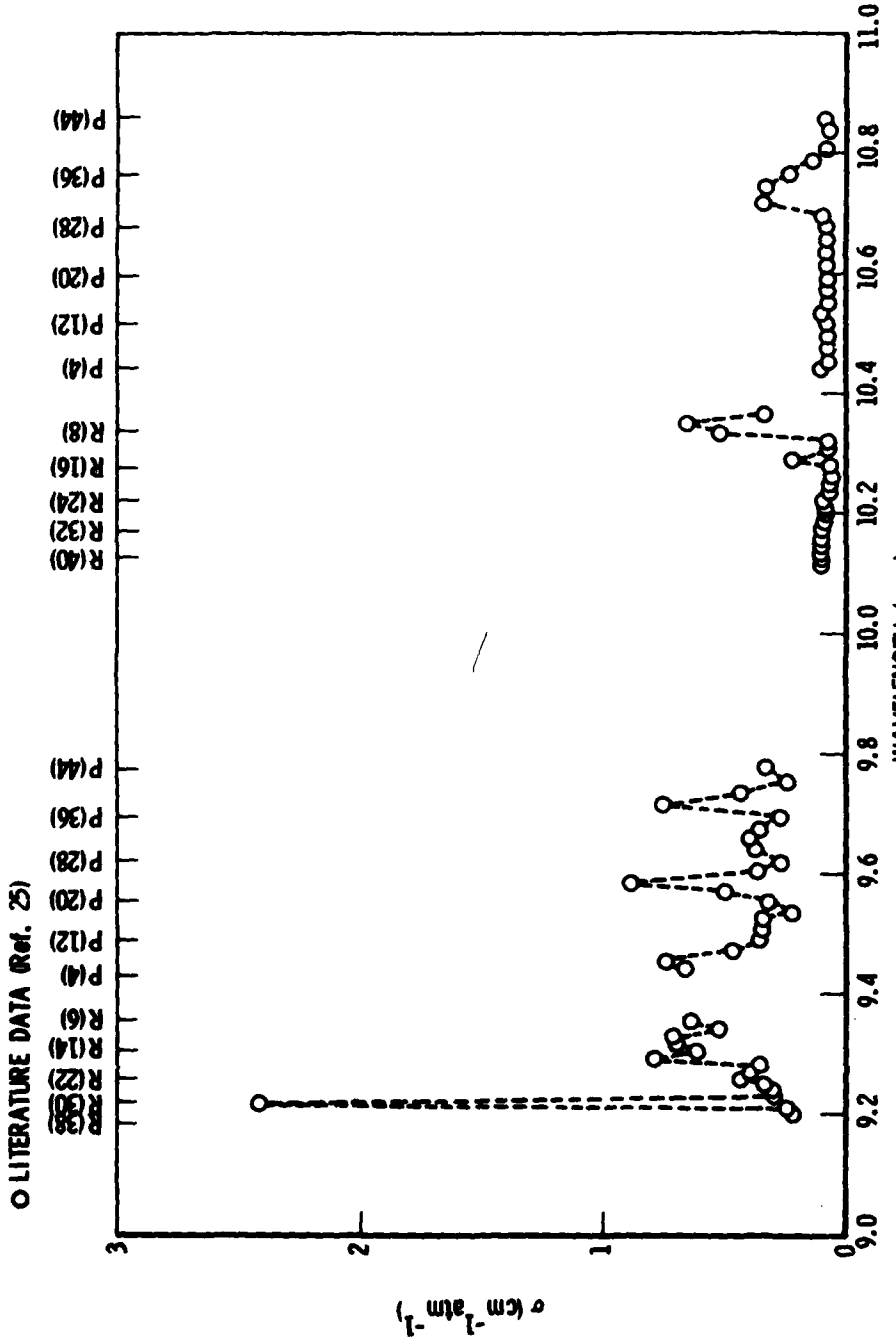

Fig. 12. $^{12}C^{16}O_2$ Laser Absorption Spectrum of Methylamine

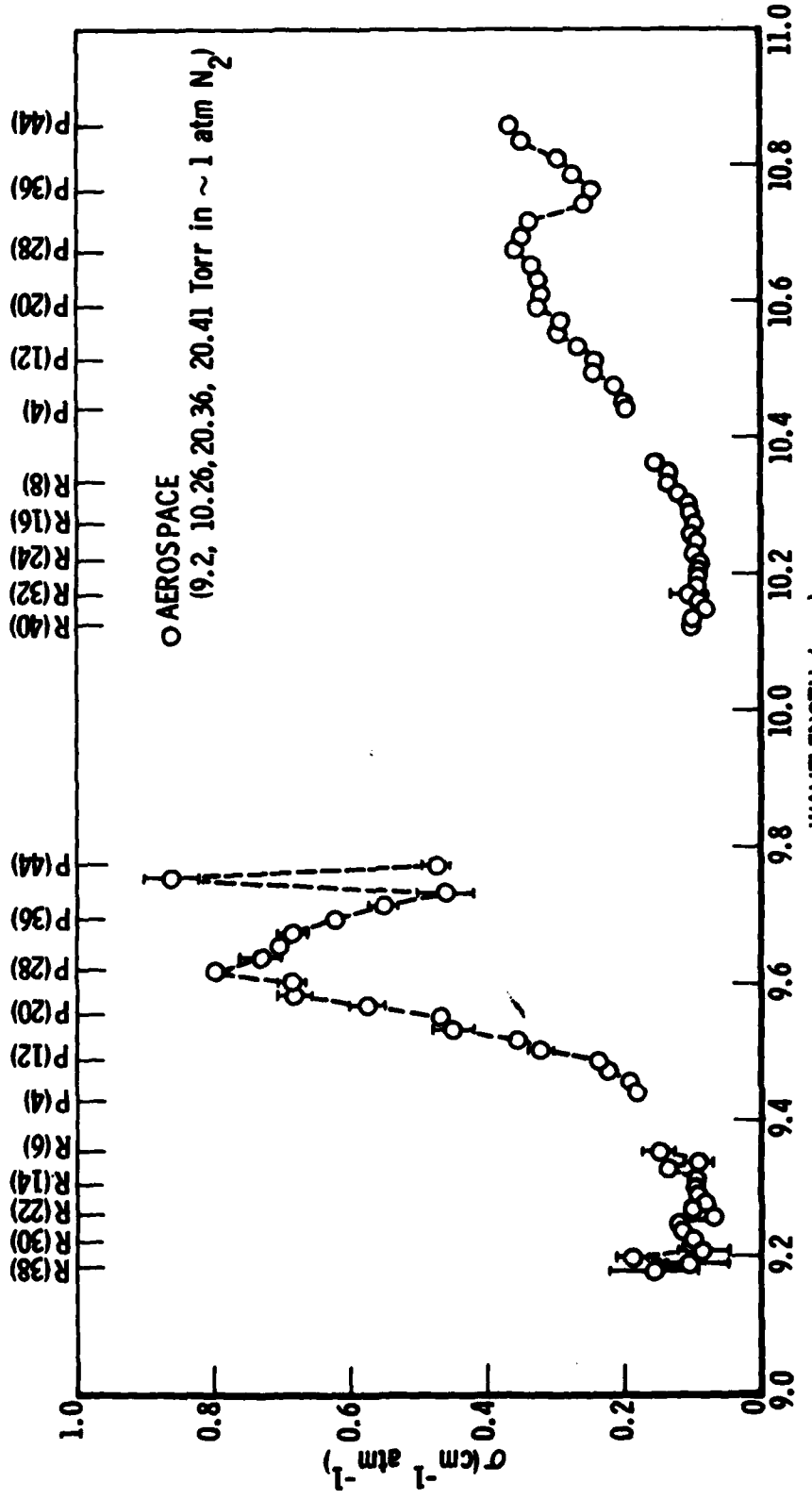

Fig. 13. $^{12}C^{16}O_2$ Laser Absorption Spectrum of Dimethylamine

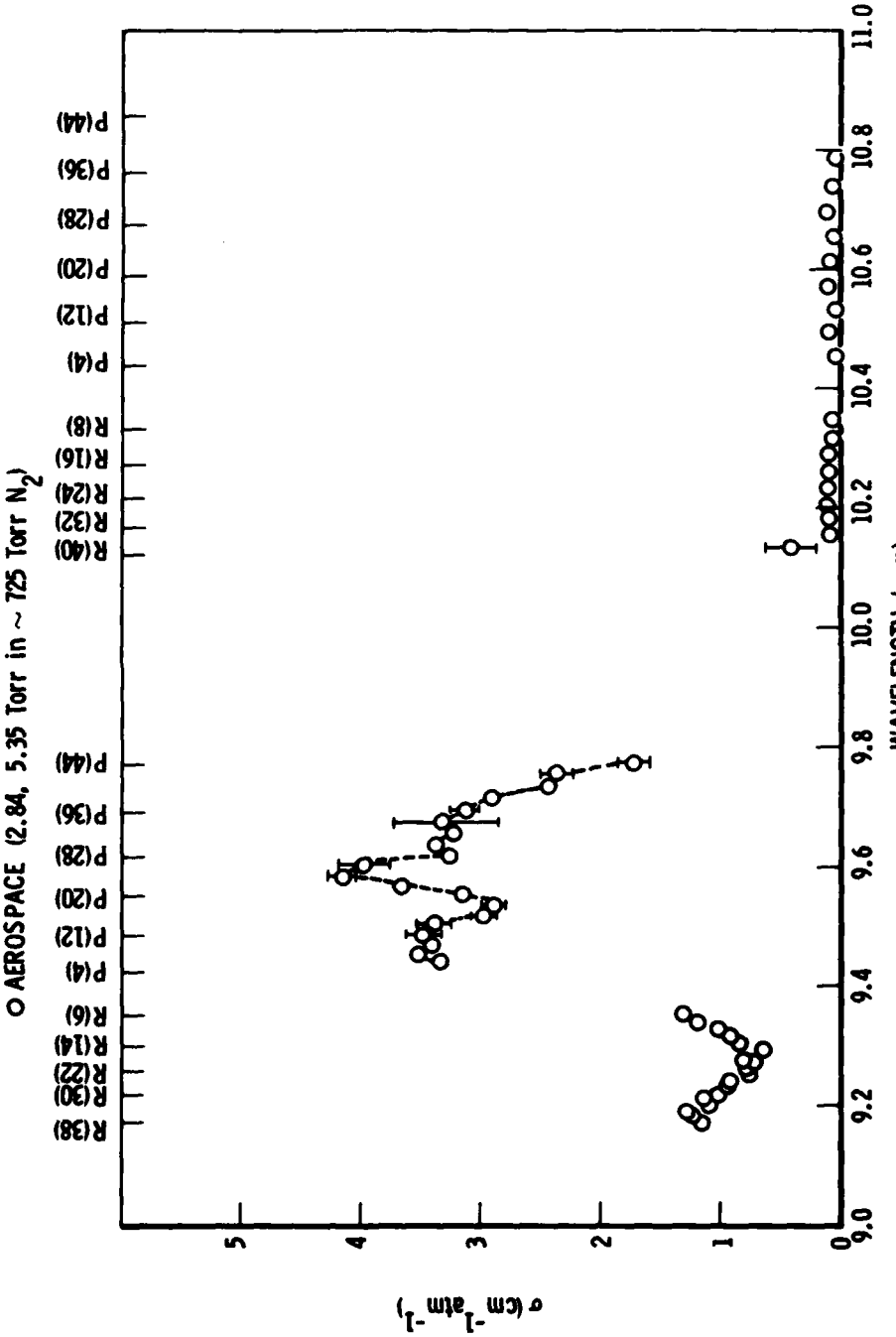

Fig. 14. $^{12}C^{16}O_2$ Laser Absorption Spectrum of Trimethylamine

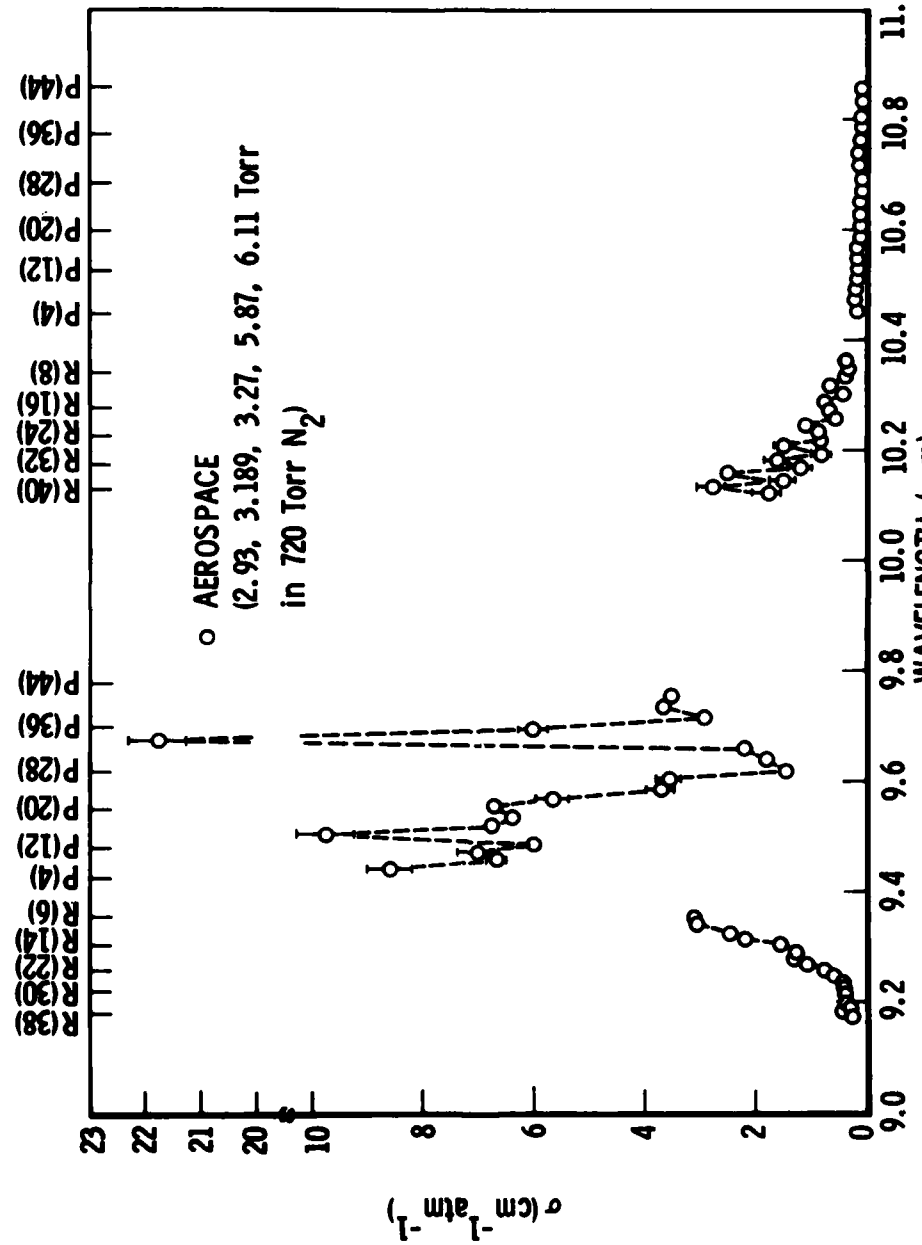

Fig. 15. $^{12}C^{16}O_2$ Laser Absorption Spectrum of Methanol

Table I. Absorption Coefficients ($cm^{-1}atm^{-1}$) of Hydrazines and Some of Their Air Oxidation Products

$^{12}C^{16}O_2$ Laser 9.4μm ($00^{0}1$-$02^{0}0$) Band									
Transition	λ (μm)	Hydrazine	Monomethyl-hydrazine	Unsymmetrical dimethyl hydrazine	Ammonia[a]	Monomethyl-amine[b]	Dimethylamine	Trimethylamine	Methanol
R(40)	9.174	–	–	–	1.70	–	–	1.15	0.25 ± .10
R(38)	9.183	0.86 ± .02	–	–	0.377	–	0.14 ± .03	1.23 ± .07	0.42 ± .03
R(36)	9.192	0.67 ± .05	0.54	0.32 ± .03	0.0739	–	0.10 ± .06	1.26	0.28 ± .16
R(34)	9.201	0.45 ± .04	0.29 ± .04	0.24 ± .03	0.212	0.218	0.19 ± .02	1.12 ± .04	0.35 ± .14
R(32)	9.210	0.60 ± .06	0.35 ± .03	0.35	0.536	0.247	0.08 ± .04	1.13 ± .06	0.33 ± .07
R(30)	9.219	0.75	0.56 ± .07	0.27 ± .03	56.2	2.423	0.10 ± .01	1.03 ± .01	0.38 ± .01
R(28)	9.229	0.50 ± .03	0.31 ± .05	0.30 ± .03	0.407	0.285	0.10 ± .01	0.96 ± .03	0.40 ± .07
R(26)	9.239	0.41 ± .03	0.25 ± .03	0.35	0.0996	0.293	0.11 ± .01	0.94 ± .02	0.41 ± .05
R(24)	9.250	0.73	0.42 ± .04	0.32 ± .04	0.0583	0.328	0.12	0.76	0.59 ± .06
R(22)	9.260	0.58 ± .01	0.50 ± .02	0.38 ± .01	0.0489	0.437	0.07 ± .01	0.77 ± .01	0.76 ± .06
R(20)	9.271	0.61 ± .05	0.30	0.39 ± .03	0.0514	0.397	0.10	0.72 ± .04	1.07 ± .23
R(18)	9.282	0.50 ± .04	0.23	0.47 ± .04	0.107	0.361	0.08 ± .01	0.81 ± .01	1.30 ± .08
R(16)	9.293	0.48 ± .03	0.19	0.52 ± .01	11.2	0.786	0.09	0.65	1.24 ± .11
R(14)	9.305	0.60 ± .02	0.22 ± .02	0.65 ± .03	0.639	0.622	0.10 ± .01	0.84 ± .05	1.54 ± .01
R(12)	9.317	0.65 ± .05	0.14	0.69 ± .04	0.282	0.691	0.10	0.91 ± .02	2.18 ± .06
R(10)	9.329	0.69 ± .10	0.22 ± .10	0.67 ± .06	0.223	0.408	0.1[illegible] ± .01	1.02 ± .01	2.48 ± .07
R(8)	9.342	0.63	0.33 ± .03	0.77 ± .03	1.65	0.526	0.09 ± .02	1.19 ± .02	3.03 ± .12
R(6)	9.355	0.59 ± .01	0.02 ± .03	1.01 ± .13	0.112	0.631	0.15 ± .01	1.30 ± .05	3.09 ± .14
P(6)	9.443	0.73 ± .05	0.21 ± .03	1.41	0.143	0.676	0.18 ± .01	3.33 ± .06	8.59 ± .42
P(8)	9.458	0.61 ± .04	0.07	1.32 ± .02	0.0488	0.731	0.19 ± .01	3.50 ± .01	6.67 ± .17
P(10)	9.473	0.58 ± .03	0.17	1.26 ± .02	0.331	0.466	0.22 ± .01	3.41 ± .05	7.01 ± .37
P(12)	9.488	0.80 ± .04	0.11 ± .01	1.43	0.965	0.356	0.24 ± .02	3.47 ± .15	5.98 ± .10
P(14)	9.504	0.58 ± .02	0.15	1.54 ± .01	0.348	0.350	0.32 ± .02	3.39 ± .13	9.75 ± .52
P(16)	9.520	0.65 ± .05	0.12	1.53 ± .02	0.162	0.338	0.36 ± .01	2.97 ± .07	6.76 ± .13
P(18)	9.536	0.72 ± .01	0.16 ± .01	1.52 ± .03	0.230	0.220	0.45 ± .03	2.90 ± .08	6.37 ± .13
P(20)	9.553	0.81	0.13 ± .03	1.51 ± .02	2.93	0.318	0.47 ± .01	3.15 ± .07	3.69 ± .13
P(22)	9.569	0.58 ± .01	0.08 ± .02	1.40 ± .03	0.356	0.498	0.58 ± .01	3.66 ± .08	5.65 ± .29
P(24)	9.586	0.95 ± .02	0.12 ± .02	1.51 ± .06	0.348	0.881	0.68 ± .03	4.15	3.69 ± .26
P(26)	9.604	0.75 ± .01	0.17 ± .03	1.52 ± .01	0.0917	0.357	0.68 ± .01	3.96 ± .22	3.56 ± .22
P(28)	9.621	0.74 ± .04	0.12	1.61 ± .03	0.0545	0.269	0.80 ± .01	3.26 ± .08	1.45 ± .09
P(30)	9.639	0.54	0.10 ± .02	1.59	0.0605	0.370	0.73 ± .03	3.36 ± .06	1.80 ± .08
P(32)	9.658	0.77 ± .11	0.11 ± .01	1.69 ± .08	0.260	0.388	0.70 ± .01	3.22 ± .01	2.21 ± .05
P(34)	9.676	0.82 ± .03	0.16	1.59 ± .04	3.74	0.358	0.68 ± .02	3.25 ± .45	21.77 ± .52
P(36)	9.695	1.06 ± .05	0.04 ± .02	1.55 ± .07	0.563	0.269	0.62 ± .02	3.13 ± .12	6.01 ± .27
P(38)	9.714	0.83 ± .02	0.09 ± .05	1.49 ± .02	0.144	0.748	0.56 ± .01	2.86 ± .11	2.90 ± .05
P(40)	9.734	0.95 ± .07	0.14 ± .01	1.33 ± .07	1.76	0.427	0.45 ± .04	2.42 ± .04	3.67 ± .06
P(42)	9.753	1.06 ± .08	0.03 ± .04	1.18 ± .02	0.0965	0.248	0.86 ± .04	2.36 ± .13	3.52 ± .10
P(44)	9.774	1.05 ± .23	0.16	–	–	0.320	0.47 ± .02	1.72 ± .13	–

Table I. Absorption Coefficients ($cm^{-1}atm^{-1}$) of Hydrazines and Some of Their Air Oxidation Products (Continued)

$^{12}C^{16}O_2$ Laser 10.4 μm (00^01-10^00) Band									
Transition	λ (μm)	Hydrazine	Monomethyl-hydrazine	Unsymmetrical dimethyl hydrazine	Ammonia[a]	Monomethyl-amine[b]	Dimethylamine	Trimethylamine	Methanol
R(42)	10.114	–	1.03	–	–	0.0955	–	–	–
R(40)	10.124	1.98 ± .11	1.16 ± .11	–	0.149	0.0986	0.10 ± .01	–	1.78 ± .25
R(38)	10.135	2.76	1.09 ± .02	0.06 ± .05	0.0162	0.0952	0.10 ± .02	0.41 ± .022	2.77 ± .25
R(36)	10.147	2.43 ± .09	1.17 ± .03	0.22 ± .08	0.0125	0.0958	0.08 ± .01		1.50 ± .23
R(34)	10.158	3.06 ± .06	1.25 ± .04	0.13	0.0110	0.0914	0.09 ± .01	0.05	2.50 ± .21
R(32)	10.170	2.93 ± .03	1.28 ± .04	0.14	0.0110	0.0895	0.10 ± .03		1.19 ± .21
R(30)	10.182	3.59 ± .04	1.36 ± .09	0.04 ± .04	0.0135	0.0869	0.09 ± .01	0.09 ± .04	1.62 ± .22
R(28)	10.194	2.06 ± .02	1.35 ± .05	0.13 ± .05	0.0139	0.0754	0.09		0.81 ± .18
R(26)	10.207	2.85	1.35 ± .04	0.03	0.0150	0.0701	0.09 ± .01	0.11 ± .03	1.48 ± .16
R(24)	10.219	3.11 ± .03	1.38 ± .04	0.09	0.0186	0.0719	0.09 ± .01		0.80 ± .01
R(22)	10.233	2.92	1.21 ± .08	0.09 ± .02	0.0257	0.0681	0.09 ± .01	0.09 ± .02	0.86 ± .12
R(20)	10.247	4.87 ± .02	0.98 ± .06	0.17 ± .01	0.0355	0.0668	0.09		1.08 ± .01
R(18)	10.260	4.47	0.93 ± .02	0.09 ± .04	0.0534	0.0588	0.10 ± .01	0.08 ± .02	0.54 ± .12
R(16)	10.274	3.50 ± .01	0.92 ± .03	0.06 ± .04	0.0995	0.0661	0.10 ± .01		0.65 ± .01
R(14)	10.289	4.45	0.79 ± .03	0.12 ± .03	6.34	0.207	0.11 ± .01	0.09 ± .06	0.72 ± .10
R(12)	10.303	3.61 ± .02	0.78 ± .03	0.06 ± .02	0.230	0.0695	0.10		0.40
R(10)	10.318	3.57 ± .01	1.19 ± .03	0.05 ± .02	0.542	0.0704	0.12 ± .01	0.04	0.66 ± .06
R(8)	10.334	4.71 ± .10	3.48 ± .15	0.13 ± .03	20.5	0.514	0.14		0.37
R(6)	10.349	4.76 ± .04	0.87 ± .07	0.10 ± .04	26.3	0.644	0.13 ± .01	0.03 ± .08	0.32 ± .03
R(4)	10.365	4.73 ± .17	1.52 ± .08	0.06 ± .06	11.0	0.331	0.15 ± .01	–	0.35 ± .02
P(4)	10.441	7.56 ± .11	1.23 ± .02	–	2.00	0.0938	0.19 ± .02	–	–
P(6)	10.453	4.33 ± .05	1.35 ± .05	0.05	0.601	0.0627	0.20 ± .01	0.02 ± .07	0.16 ± .01
P(8)	10.476	3.19 ± .01	1.29 ± .05	0.12 ± .02	0.273	0.0695	0.21		0.20 ± .05
P(10)	10.494	2.82 ± .01	1.44 ± .06	0.13	0.207	0.0667	0.24	0.09	0.18
P(12)	10.513	3.45 ± .06	1.30 ± .07	0.16 ± .03	0.663	0.0706	0.24		0.17 ± .02
P(14)	10.532	5.31 ± .05	1.28 ± .04	0.16 ± .01	0.795	0.0872	0.27	0.02 ± .03	0.13
P(16)	10.551	4.21 ± .03	1.24 ± .05	0.27 ± .03	0.541	0.0655	0.30 ± .01		0.14 ± .02
P(18)	10.571	2.65	1.12 ± .01	0.28 ± .02	0.166	0.0629	0.30 ± .01	0.08 ± .01	0.17 ± .01
P(20)	10.591	4.57 ± .05	1.18 ± .02	0.40 ± .02	0.143	0.0651	0.33 ± .01		0.10
P(22)	10.611	5.41	1.00 ± .01	0.44	0.0808	0.0643	0.32	0.06 ± .08	0.10 ± .03
P(24)	10.632	4.56 ± .01	1.03 ± .01	0.56 ± .04	0.140	0.0658	0.33 ± .01		0.11 ± .02
P(26)	10.653	4.68 ± .03	1.03	0.64 ± .02	0.369	0.0660	0.33	0.01 ± .02	0.10 ± .01
P(28)	10.674	2.17	1.06 ± .04	1.11 ± .02	0.332	0.0690	0.37 ± .01		0.04 ± .02
P(30)	10.696	2.65 ± .01	1.01 ± .01	1.45 ± .04	0.922	0.0819	0.35	0.08 ± .02	0.04
P(32)	10.718	6.18 ± .01	1.14 ± .02	1.86 ± .04	13.7	0.358	0.33		0.11 ± .01
P(34)	10.741	4.48 ± .04	1.18 ± .04	2.40 ± .01	14.0	0.354	0.26 ± .01	0.04	0.13 ± .04
P(36)	10.764	2.44 ± .03	1.23 ± .05	2.88 ± .05	8.43	0.223	0.25		0.09 ± .03
P(38)	10.787	3.16 ± .03	1.29 ± .02	3.27 ± .13	4.21	0.135	0.27 ± .01	0.01	0.07 ± .04
P(40)	10.810	7.45 ± .06	1.46 ± .02	3.59 ± .14	0.950	0.0784	0.29 ± .01		0.08 ± .02

Table I. Absorption Coefficients ($cm^{-1}atm^{-1}$) of Hydrazines and Some of Their Air Oxidation Products (Continued)

$^{12}C^{16}O_2$ Laser 10.4 μm ($00^{0}1$-$10^{0}0$) Band Transition	λ (μm)	Hydrazine	Monomethyl-hydrazine	Unsymmetrical dimethyl hydrazine	Ammonia[a]	Monomethyl-amine[b]	Dimethylamine	Trimethylamine	Methanol
P(42)	10.834	4.17 ±.09	1.54 ± .01	3.95 ± .14	0.412	0.0685	0.35		0.08 ± .04
P(44)	10.858	2.81 ±.01	1.70 ± .05	3.95 ± .23	–	0.0766	0.37		0.08 ± .01
P(46)	10.883	3.41 ±.02	2.06 ± .05	3.90 ± .08	–		–		–

[a] Ref. 24 - Average error ± 6.14%

[b] Ref. 25

A. $^{12}C^{16}O_2$ LASER ABSORPTION SPECTRA OF THE HYDRAZINE-HYDRAZINE-BASED ROCKET FUELS

1. HYDRAZINE

The hydrazine high-resolution absorption spectrum in Fig. 8 consists of weak absorption throughout the 9.4-μm $^{12}C^{16}O_2$ laser band, but a series of very distinct peaks and valleys within the P and R branches of the 10.4-μm band. Approximately half the 10.4-μm $^{12}C^{16}O_2$ laser lines are absorbed by hydrazine with cross sections greater than 3.5 cm^{-1} atm^{-1}, and three of the lines (P4, P32, and P40) are absorbed with cross sections greater than 6.0 cm^{-1} atm^{-1}.

The data points represented by circles in Fig. 8 were determined with the Aerospace-assembled laser. A complete spectrum was first recorded by taking the average of generally three or more absorption cross-section measurements at each laser line with the use of a sample of 3.21 Torr of hydrazine buffered to a total pressure of 760 Torr with nitrogen. A partial replicate spectrum was recorded with 3.18 Torr of hydrazine for the laser wavelengths 9.658 (P32) to 9.774 μm (P44) and for alternate laser lines from 10.124 (R40) to 10.365 μm (R4) and 10.441 (P4) to 10.858 μm (P44). Averages of the 3.21- and 3.18-Torr hydrazine absorption data are plotted where these replicate measurements were made. Except where otherwise noted, the disagreement between the 3.21- and 3.18-Torr hydrazine absorption cross sections and/or the uncertainty in the cross-section measurements at either pressure were less than the size of the data point symbol.

The data points represented by squares in Fig. 8 correspond to measurements made with the Sylvania laser. For the 10.4-μm P and R branch measurements, two different hydrazine pressures (0.956 and 0.995 Torr) were employed. The P20 to P32 portion of the 10.4-μm absorption was rechecked with 1.040 Torr of hydrazine. The uncertainties associated with these hydrazine data points, determined at low hydrazine pressures, are much larger (and the data therefore less reliable) than the cross sections determined at higher hydrazine pressures with the Aerospace-

assembled laser. Similar observations can be made for the MMH and UDMH absorption data. The absorption cross sections given for the hydrazines in Table I correspond to those measured with the Aerospace-assembled laser only. Even with the large uncertainties in the hydrazine data determined with the Sylvania laser, there is good general agreement between the absorption cross sections determined by the two laser systems.

The highly structured features observed in the hydrazine spectrum in Fig. 8 should serve as a unique spectral fingerprint to permit highly specific detection of hydrazine by CO_2 laser spectroscopy.

2. MMH

The MMH high-resolution absorption spectrum in Fig. 9 consists of weak absorption in the 9.2- to 9.8-μm wavelength region and moderate absorption in the 10.1- to 10.9-μm region. A sharp MMH absorption feature with a cross section close to 3.5 $cm^{-1}atm^{-1}$ is observed at the 10.334-μm (R8) $^{12}C^{16}O_2$ laser line.

The data points designated by circles in Fig. 9 were determined with the Aerospace-assembled laser. The absorption data plotted over the $^{12}C^{16}O_2$ laser 10.4-μm band represent averages of absorption measurements made on samples of 2.87 and 6.01 Torr of MMH. The MMH absorption data for the $^{12}C^{16}O_2$ laser 9.4-μm band P and R branches were determined during the 2.87- and 6.01-Torr MMH spectral measurements, respectively. The uncertainties in these absorption cross sections are (as for most of the absorption cross sections measured with the Aerospace-assembled laser) generally smaller than the size of the data symbols, i.e., less than approximately ±7%.

The MMH absorption cross sections determined with the Sylvania laser are represented by squares in Fig. 9. The $^{12}C^{16}O_2$ laser 10.4-μm P-branch MMH absorption data represent averages of absorption measurements made with the use of MMH pressures of 2.00, 2.01, and 2.99 Torr. The 10.4-μm R-branch measurements were performed on the 2.01- and

2.99-Torr samples. Good general agreement can be observed between the MMH absorption cross sections determined with the Aerospace-assembled laser and the Sylvania laser.

3. UDMH

The high-resolution absorption spectrum for UDMH in Fig. 10 shows absorption maxima of about 1.5 $cm^{-1}atm^{-1}$ and 4.0 $cm^{-1}atm^{-1}$ within the $^{12}C^{16}O_2$ laser 9.4- and 10.4-μm bands, respectively.

The data points designated by circles were determined with the Aerospace-assembled laser. Absorption in the 9.4-μm $^{12}C^{16}O_2$ laser band was determined using 4.88 Torr of UDMH, and absorption in the 10.4-μm band was determined on 5.06 Torr of UDMH. Absorption cross sections determined on the 4.88-Torr UDMH sample at four separate laser lines (R38, P10, P42, P44) in the 10.4-μm band were in good agreement with the corresponding 5.06-Torr data.

The absorption cross sections designated by squares in Fig. 10 represent averages of absorption measurements made at 1.85 and 5.12 Torr UDMH with the Sylvania laser. The error bars associated with these data points represent the spread between the 1.85- and 5.12-Torr data. The upper limits of these error bars correspond to the 1.85-Torr measurements. These 1.85-Torr absorption cross-section data appear anomalously high compared to the other UDMH absorption data. The lower limits of these error bars correspond to the 5.12-Torr measurements. Because of the larger fraction of light absorbed with higher sample pressures, the 5.12-Torr measurements are considered more accurate than the 1.85-Torr measurements. The 5.12-Torr UDMH absorption data are in best agreement with the data determined with the Aerospace-assembled laser.

It is evident from Figs. 8 through 10 that hydrazine, MMH, and UDMH possess highly characteristic $^{12}C^{16}O_2$ laser absorption profiles. The $^{12}C^{16}O_2$ laser absorption profiles of the possible atmospheric degradation products of the hydrazines, ammonia, methylamine, dimethylamine, trimethylamine, and methanol, are described below. The expected

specificities of detecting each of the hydrazines in the presence of possible interferences are described in Section V.

B. $^{12}C^{16}O_2$ LASER ABSORPTION SPECTRA OF SELECTED HYDRAZINE FUEL DEGRADATION PRODUCTS

The absorption measurements reported here for dimethylamine, trimethylamine, and methanol were made with the Aerospace-assembled laser. Absorption measurements from the literature are presented for both ammonia and methylamine.

1. AMMONIA

High resolution $^{12}C^{16}O_2$ laser absorption spectra have been reported for ammonia in four studies.[24-27] The results obtained by these different groups are presented in Fig. 11. The data obtained by Brewer and Bruce,[24] Crane,[25] and Patty et al.[26] are in good general agreement with each other. The ammonia absorption data obtained by Mayer et al.[27] differs from those of the other groups, particularly within the P-branch of the 9.4-μm laser band and at line P8 of the 10.4-μm laser band. These differences may be in part a result of mislabelling of the absorption data according to laser line transitions by Mayer et al. The ammonia absorption cross sections determined by Brewer and Bruce are believed to be the most accurate published to date. These are the data presented in Table I.

The $^{12}C^{16}O_2$ laser high-resolution absorption spectrum for ammonia obtained by Brewer and Bruce is characterized by very highly structured peaks and valleys. Strong absorption features with cross sections of approximately 60 $cm^{-1}atm^{-1}$ and 11 $cm^{-1}atm^{-1}$ can be observed at the R30 and R16 lines of the 9.4-μm laser band. Within the 10.4-μm laser band, strong absorption features are observed at the laser lines R8 (~17 cm^{-1} atm^{-1}), R6 (~21 $cm^{-1}atm^{-1}$), and R4 (~10 $cm^{-1}atm^{-1}$).

Limited absorption measurements for ammonia within the $^{12}C^{16}O_2$ laser 10.4-μm band, made with the Sylvania laser, were found to be in good agreement with the data of Brewer and Bruce,[24] Crane,[25] and Patty et al.[26]

2. METHYLAMINE

The $^{12}C^{16}O_2$ laser high-resolution absorption data for methylamine presented in Fig. 12 were determined by Crane.[25,28] Comparison of the spectrum in Fig. 12 with that for ammonia[24] in Fig. 11 indicates that ammonia may have been present as an impurity at the 3 to 4% level in Crane's[25,28] methylamine sample. Some of the strongest absorption features observed in the spectrum in Fig. 12 are identical with the strongest features observed in Fig. 11 for ammonia.[24] This is particularly true at the $^{12}C^{16}O_2$ laser 9.4-μm band R30 and R16 lines, and at the R8 through R4 and P32 through P36 lines in the 10.4-μm laser band. The relative ammonia absorption intensity ratios of the laser lines within the 10.4-μm $^{12}C^{16}O_2$ laser band in Fig. 11 are: R8/R6/R4≈0.80/1.00/0.51 and P32/P34/P36≈1.00/0.99/0.62. The corresponding ratios in Fig. 12 are: R8/R6/R4 ≈ 0.80/1.00/0.46 and P32/P34/P36≈1.00/0.97/0.58. It thus appears that the methylamine $^{12}C^{16}O_2$ laser absorption spectrum should be redetermined on a methylamine sample from which ammonia impurities have been carefully removed. Crane's methylamine data in Table I should be considered preliminary and subject to revision.

3. DIMETHYLAMINE

The data in Fig. 13 indicate that dimethylamine possesses absorption bands within both the 9.4- and 10.4-μm $^{12}C^{16}O_2$ laser bands. Absorption peaks with maxima of approximately 0.80 $cm^{-1}atm^{-1}$ and 0.86 $cm^{-1}atm^{-1}$, respectively, are observed at the P28 and P42 lines within the 9.4-μm laser band. An absorption valley occurs at the P40 line within the 9.4-μm laser band. Within the 10.4-μm laser band, dimethylamine has absorption maxima of approximately 0.36 $cm^{-1}atm^{-1}$ near the P28 and P46 laser lines and an absorption valley of approximately 0.25 $cm^{-1}atm^{-1}$ at the P36 laser line.

Different pressures were used to determine the absorption cross sections for dimethylamine in each branch of the $^{12}C^{16}O_2$ laser output. Absorption measurements throughout the R and P branches of the 9.4-μm

laser band were carried out with 9.20 and 10.25 Torr of dimethylamine, respectively. Pressures of 20.36 and 20.51 Torr of dimethylamine were used for the 10.4-μm laser band R- and P-branch absorption measurements, respectively. The dimethylamine absorption measurements were cross-checked at selected $^{12}C^{16}O_2$ laser wavelengths with different dimethylamine pressures. These measurements were carried out over the 9.4-μm laser band with the use of the following laser lines and dimethylamine pressures: R10 and R6 (10.25 Torr); alternate lines from P10 to P38, P40 and P42 (20.36 Torr); P38 to P42 (9.20 Torr); and P40 to P44 (20.41 Torr). Absorption measurements that were cross-checked over the 10.4-μm laser band included: R14, R10, R8, R4 (20.41 Torr); R40 to R28 (10.25 Torr); and P4 and P28 (20.36 Torr). The data point uncertainty at laser wavelengths where multiple absorption measurements were made is observed in Fig. 13 to be small.

4. TRIMETHYLAMINE

Figure 14 indicates that trimethylamine absorbs negligibly within the 10.4-μm $^{12}C^{16}O_2$ laser band, but possesses moderate absorption within the 9.4-μm laser band. Trimethylamine absorption within the 9.4-μm $^{12}C^{16}O_2$ laser band is characterized by absorption shoulders with cross sections approximately 3.5 $cm^{-1}atm^{-1}$ and 3.3 $cm^{-1}atm^{-1}$ near the laser lines P8 to P12 and P28 to P34, respectively, and by a central absorption peak with a cross section of about 4.0 $cm^{-1}atm^{-1}$ near the P24 and P26 laser lines. Distinct absorption valleys are observed at the R24 to R14 and P16 and P18 laser lines.

The absorption data in the 9.4-μm laser band in Fig. 14 were determined over the laser lines R36 to R6 and P6 to P44 with the use of 2.84 Torr of trimethylamine, and over the lines R38 to R26, R22 to R18, and P6 to P42 with the use of 5.35 Torr of trimethylamine. Absorption of selected 10.4-μm laser lines was determined with 2.84 Torr of trimethylamine.

5. METHANOL

Figure 15 shows that methanol possesses absorbances of moderate strength in the R branches of the $^{12}C^{16}O_2$ 9.4- and 10.4-μm laser bands and strong, structured absorption features in the P branch of the 9.4-μm laser band. Negligible absorption is observed for methanol over the P-branch of the $^{12}C^{16}O_2$ laser 10.4-μm band. Sharp, strong absorption features, with cross sections of approximately 8.4, 9.4, and 21.8 $cm^{-1}atm^{-1}$, are observed for methanol at the P6, P14, and P34 lines of the $^{12}C^{16}O_2$ laser 9.4-μm band.

The absorption data for methanol in the $^{12}C^{16}O_2$ laser 9.4-μm band in Fig. 15 were determined with the use of the following laser lines and methanol pressures: R40 to R6 and P36 to P40 (3.19 Torr); R36 to R6 and P6, P8, P24, and P34 (6.11 Torr); P6 to P34 (2.93 Torr); P6 to P42 (3.27 Torr); and P14, P22, P26, P30, P34, and P36 (5.87 Torr). Methanol absorption data in the $^{12}C^{16}O_2$ laser 10.4-μm band were determined over the laser lines R40 to R26 and for alternate lines from R22 to R10 with the use of 3.27 Torr of methanol, and from R40 to R4 and P6 to P44 with the use of 5.87 Torr of methanol.

V. DISCUSSION

Several factors determine the lowest levels at which selected compounds can be detected by CO_2 laser spectroscopic techniques, within prescribed confidence limits, in a multicomponent mixture. These factors, some of which are interdependent, include: (1) the sensitivity or minimum detectable absorptivity α_{min} of the particular CO_2 laser detection technique employed, (2) the absorptivities and the spectral uniqueness of both the compounds of interest and of interferences, (3) the total number of compounds that absorb within the wavelength regions of CO_2 laser output, (4) the wavelengths and number of CO_2 laser lines used for monitoring, and (5) the output power of the laser at each of these lines when the photoacoustic technique is employed.

Subsection A describes the state-of-the-art sensitivities of the CO_2 laser-based photoacoustic, long-path absorption, and lidar detection techniques. These sensitivity values are used with the absorption data from Section IV to calculate the detectabilities of the hydrazines and their degradation products studied when each is alone. The use of detection sensitivity values and absorption data to calculate expected detectabilities of various compounds in multicomponent mixtures is more complicated. In Section V. B, approximations are made of the expected detectabilities of the hydrazines in the presence of possible interferences by each $^{12}C^{16}O_2$ laser detection technique under consideration. A mathematical procedure outlined in the appendix can be used to more exactly determine the minimum spectroscopically detectable concentrations of various species in multicomponent mixtures.

A. EXPECTED INTERFERENCE-FREE DETECTABILITIES OF THE HYDRAZINES AND THEIR SELECTED OXIDATION BY $^{12}C^{16}O_2$ LASER-BASED DETECTION TECHNIQUES

1. PHOTOACOUSTIC DETECTION

The sensitivity of minimum detectable absorptivity α_{min}, obtainable

with a photoacoustic detection system for a signal-to-noise ratio of unity, is

$$\alpha_{min} = \frac{n_e}{R} \qquad (2)$$

where n_e is the total instrument noise voltage and R is the detector responsivity (V-cm W^{-1})[28]. Photoacoustic instrumentation development has been directed at maximizing the detector responsivity and minimizing the total instrument noise voltage. To increase detector responsivity, acoustically resonant photoacoustic cells have been designed to increase the amplitude of the sound signal in the cells.[29] Low-noise microphones or pressure transducers and lock-in detection techniques are generally used to minimize background signals that contribute to instrument noise. An important contributor to total instrument noise is the small amount of absorption that occurs at the windows of the photoacoustic cell independent of the absorbing gas concentration. Photoacoustic cells for which window absorption effects are minimized are being designed. This has primarily included the design of photoacoustic cells with: (1) carefully matched tandem reference and sample chambers to permit sample chamber window absorption to be nulled out with that of the reference chamber[30] and/or (2) acoustic dampers inside the cell to minimize transmission of window-absorption signals to the cell microphone.[31] Windowless photoacoustic cells are also being investigated.[32]

The most sensitive photoacoustic detector reported to date[33] has a minimum detectable absorptivity of 10^{-11} cm^{-1} W. This photoacoustic detector makes use of a rectangular waveguide cell that is best suited for use with lasers that produce a rectangular cross-section mode structure. The sensitivities of detectors suitable for use with most CO_2 lasers and other lasers that produce a circular cross-section beam are currently[30] approximately 10^{-9} cm^{-1} W. The latter sensitivity value can be used to estimate the expected minimum concentration values that can be detected by CO_2 laser photoacoustic techniques for various vapors under interference-free conditions. This is accomplished by use of the relationship

$$P_{min} = \frac{\alpha_{min}}{\sigma(\lambda)} \qquad (3)$$

where p_{min} is the minimum detectable concentration in units of atm-W, and $\sigma(\lambda)$ is the absorption cross section in units of $cm^{-1}atm^{-1}$ of the vapor of interest at the $^{12}C^{16}O_2$ laser monitoring wavelength. In the absence of interferences, the lowest detection limit of a molecule is obtained at the $^{12}C^{16}O_2$ laser wavelength where the product of the laser output power and the molecule's absorption cross section are largest. (The minimum detectable concentration value decreases linearly with increasing laser power).* The output power available at various $^{12}C^{16}O_2$ laser wavelengths is dependent on the laser used. Thus, p_{min} values (in units of atm-W) are listed at selected $^{12}C^{16}O_2$ laser wavelengths in Table II for the hydrazines and the selected air oxidation products of the hydrazines for which absorption cross-section data are presented in Section IV. Table II shows that the $^{12}C^{16}O_2$ laser-based photoacoustic detection technique should provide interference-free detectabilities of hydrazine, MMH, and UDMH of 0.2, 0.3, and 0.3 ppb, respectively, when the $^{12}C^{16}O_2$ laser excitation line used has an output power of 1 W. The other compounds in Table II should also be detectable alone at ppb levels or less by this technique.

2. LONG-PATH ABSORPTION DETECTION

The sensitivities or minimum detectable absorptivities of long-path absorption detection techniques depend on the ability to measure small differences δ in the intensities of the laser light incident on, and transmitted through, the air sample of interest. The minimum value of δ in an optimized detection system may be 0.5%. A practical value for the absorption path length ℓ in a multipass detection cell is 100 m.[34] The interference-free detection limit p'_{min} (at a signal-to-noise ratio of unity) of a given compound by long-path absorption techniques is thus estimated from Eq. (1) as follows:

$$p'_{min} = \frac{\ell \, n \, (1.000/0.995)}{\sigma(\lambda) \cdot 10^4 \text{ cm}} \qquad (4)$$

*This is valid only for laser powers below that required to saturate the absorbing transition.

Table II. Estimated Interference-Free Detection Limits for Hydrazine Fuels and Their Oxidation Products Using $^{12}C^{16}O_2$ Laser Photoacoustic Detection

Compound	$^{12}C^{16}O_2$ Laser Wavelength		$\alpha(\lambda)^a$	$\alpha_{min}/\sigma(\lambda)^b$
	$\lambda(\mu m)$	Transition	$(cm^{-1}atm^{-1})$	(atm·W)
Hydrazine	10.441	P(4)	7.56	1.3×10^{-10}
	10.718	P(32)	6.18	1.6×10^{-10}
	10.810	P(40)	7.45	1.3×10^{-10}
Monomethylhydrazine	10.334	R(8)	3.48	2.9×10^{-10}
	10.858	P(44)	1.70	5.9×10^{-10}
	10.883	P(46)	2.06	4.9×10^{-10}
Unsymmetrical dimethylhydrazine	10.810	P(40)	3.59	2.8×10^{-10}
	10.834	P(42)	3.95	2.5×10^{-10}
	10.858	P(44)	3.95	2.5×10^{-10}
	10.883	P(46)	3.90	2.6×10^{-10}
Ammonia	9.219	R(30)	56.2	1.8×10^{-11}
	10.334	R(8)	20.5	4.9×10^{-11}
	10.349	R(6)	26.3	3.8×10^{-11}
Monomethylamine[c]	9.458	P(8)	0.731	1.4×10^{-9}
	9.586	P(24)	0.881	1.1×10^{-9}
	9.714	P(38)	0.748	1.3×10^{-9}
Dimethylamine	9.621	P(28)	0.80	1.3×10^{-9}
	9.639	P(30)	0.73	1.4×10^{-9}
	9.753	P(42)	0.86	1.2×10^{-9}
Trimethylamine	9.569	P(22)	3.66	2.7×10^{-10}
	9.586	P(24)	4.15	2.4×10^{-10}
	9.604	P(26)	3.96	2.5×10^{-10}
Methanol	9.443	P(6)	8.59	1.2×10^{-10}
	9.504	P(14)	9.75	1.0×10^{-10}
	9.676	P(34)	21.77	4.6×10^{-11}

[a]Uncertainties for absorption cross-section data given in Table I.

[b]Assumes an α_{min} value of 10^{-9} cm^{-1}· W.

[c]Absorption due to suspected ammonia impurities in methylamine spectrum of Fig. 12 are not considered here.

The estimated interference-free detection limits for the hydrazines and some of their degradation products by the long-path absorption technique are listed in Table III. It is apparent, when Tables II and III are compared, that long-path absorption techniques, which use a 100-m path length cell and a detector capable of measuring light intensity differences down to 0.5%, would provide interference-free detection limits approximately 500 times higher than expected with a photoacoustic detector in conjunction with a $^{12}C^{16}O_2$ line-tunable laser source of 1-W power. Such long-path absorption detection techniques would permit detection of hydrazine, MMH, and UDMH at levels of approximately 70, 140, and 130 ppb, respectively.

3. LIDAR DETECTION

Lidar techniques have the potential for remote detection of hydrazine fuels and their toxic degradation products.[35] The laser transmitter can be pointed in any direction and thus provide a three-dimensional profile of the toxic vapors of concern. Lidar detection techniques complement the point-sampling capabilities of photoacoustic detection and conventional absorption detection carried out with a long-path multipass cell. However, lidar systems are more costly and more technically complex than photoacoustic and conventional long-path absorption detection techniques.

Lidar detection methods may incorporate one of several different processes by which light is scattered from molecules for the measurement of these species. A full description of various lidar techniques is given in Ref. 35. The method most suitable for toxic vapor detection with CO_2 lasers is differential absorption scattering lidar.[35]

This technique, as most commonly employed (Fig. 16), uses at least two pulsed laser beams at slightly different wavelengths and a detector capable of monitoring the intensity of backscattered radiation from aerosols as these beams propagate through the atmosphere. These beams are sequentially or simultaneously transmitted along the same atmospheric path. The wavelength λ_r of one laser beam is chosen to coincide with an absorption peak of the molecule of interest, while the

Table III. Estimated Interference-Free Detection Limits for Hydrazine Fuels and Their Oxidation Products Using $^{12}C^{16}O_2$ Laser Long-Path Absorption Detection

Compound	CO_2 Laser Wavelength		$\sigma(\lambda)^a$	Estimated Minimum Detectable Concentration, p'_{min}[c]
	$\lambda(\mu m)$	Transition	$(cm^{-1}atm^{-1})$	(atm)
Hydrazine	10.441	P(4)	7.56	6.6×10^{-8}
	10.718	P(32)	6.18	8.1×10^{-8}
	10.810	P(40)	7.45	6.7×10^{-8}
Monomethylhydrazine	10.334	R(8)	3.48	1.4×10^{-7}
	10.858	P(44)	1.70	2.9×10^{-7}
	10.883	P(46)	2.06	2.4×10^{-7}
Unsymmetrical dimethylhydrazine	10.810	P(40)	3.59	1.4×10^{-7}
	10.834	P(42)	3.95	1.3×10^{-7}
	10.858	P(44)	3.95	1.3×10^{-7}
	10.883	P(46)	3.90	1.3×10^{-7}
Ammonia	9.219	R(30)	56.2	8.9×10^{-9}
	10.334	R(8)	20.5	2.4×10^{-8}
	10.349	R(6)	26.3	1.9×10^{-8}
Monomethylamine[c]	9.458	P(8)	0.731	6.8×10^{-7}
	9.586	P(24)	0.881	5.7×10^{-7}
	9.714	P(38)	0.748	6.7×10^{-7}
Dimethylamine	9.621	P(28)	0.80	6.3×10^{-7}
	9.639	P(30)	0.73	6.9×10^{-7}
	9.753	P(42)	0.86	5.8×10^{-7}
Trimethylamine	9.569	P(22)	3.66	1.4×10^{-7}
	9.586	P(24)	4.15	1.2×10^{-7}
	9.604	P(26)	3.96	1.3×10^{-7}
Methanol	9.443	P(6)	8.59	5.8×10^{-8}
	9.504	P(14)	9.75	5.1×10^{-8}
	9.676	P(34)	21.77	2.3×10^{-8}

[a]Uncertainties for absorption cross-section data given in Table I.

[b]Assumes a δ value of 0.5% and a path length of 100 meters [see Eq. (4) text].

[c]Absorption due to suspected ammonia impurities in methylamine spectrum of Fig. 12 are not considered here.

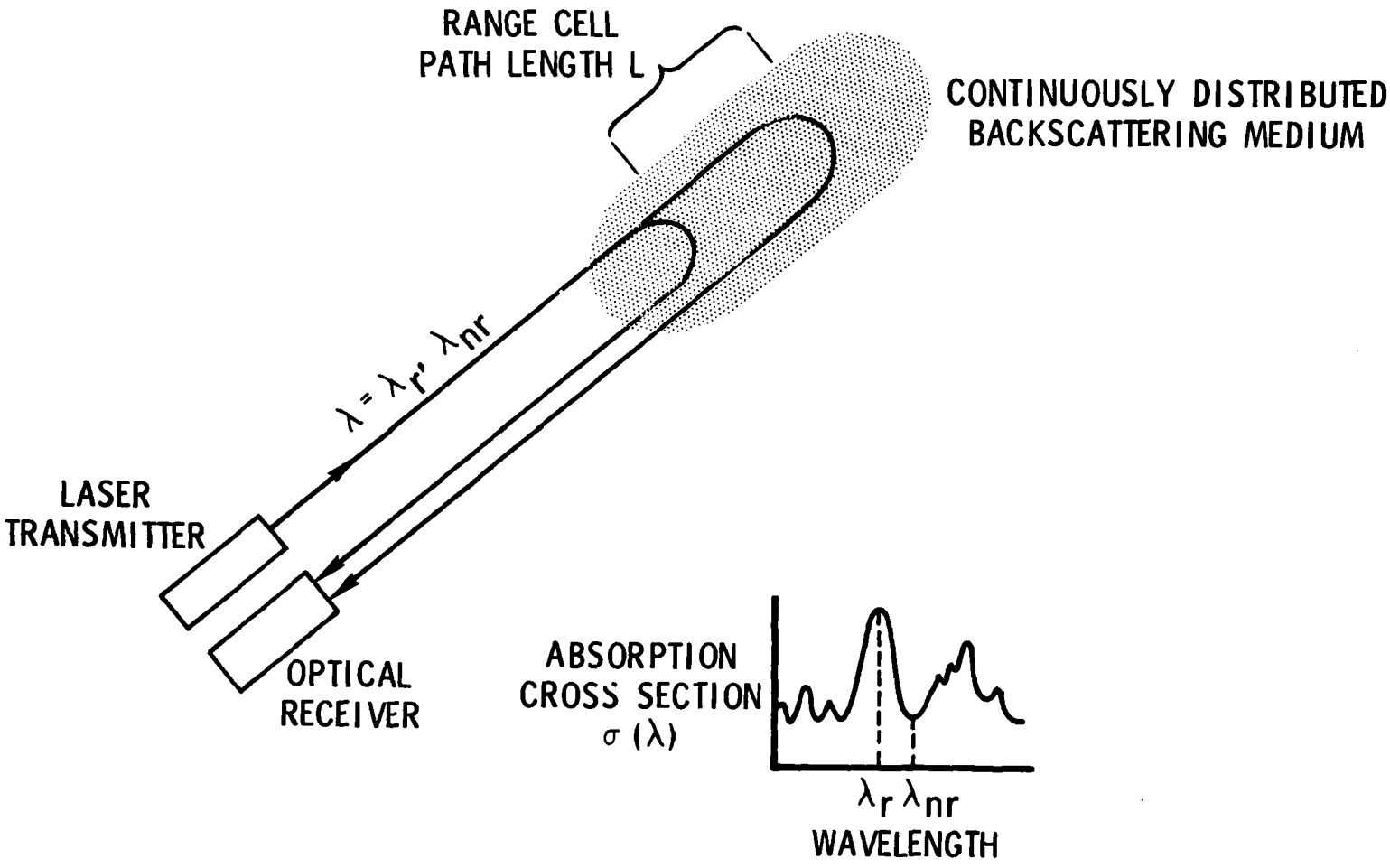

Fig. 16. Differential Absorption Lidar Technique

wavelength λ_{nr} of the other is chosen at an absorption minimum. Because the beams differ only slightly in wavelength, aerosol scattering is nearly the same for both. The difference in scattered intensities of the two beams as they propagate through the atmosphere is a result of the difference in absorption by the molecule of interest at the two wavelengths. Range-resolved information on the concentrations of airborne molecules can be obtained by analysis of the scattered light intensities of each beam as a function of time.

The detection sensitivity of lidar techniques depends on the ability to monitor small changes in the receiver power, not on the magnitude of the receiver power itself, provided sufficient scattered power is available at the detector. The transmitted power, however, determines the range over which the method can be used. For all detection configurations under consideration, sufficient laser transmitter power is available at the desired CO_2 laser wavelengths. If δ represents the smallest difference in power that can be measured between the two pulse pairs, the minimum detectable concentration n_{min} is given by

$$n_{min} = \delta/2\Delta\alpha L \qquad (5)$$

where $\Delta\alpha$ is the differential absorption $\alpha_r - \alpha_{nr}$ and L is the range cell length in Fig. 16.

For remote monitoring of hydrazine fuels and their atmospheric degradation products over a wide area, a typical range cell path length of L = 100 m might be used. As in the case of the long-path absorption technique, an optimized value for δ is assumed to be 0.5%. Using these values, the expected interference-free $^{12}C^{16}O_2$ laser-based detection limits (at a signal-to-noise ratio of 1) of various molecules can be calculated from Eq. (5) if the $^{12}C^{16}O_2$ laser absorption cross sections of these species are known. The expected lidar detection limits calculated for the hydrazines and their degradation products are listed in Table IV. The detection limits for the three hydrazines vary between 20 and 90 ppb.

Table IV. Estimated Interference-Free Detection Limits for Hydrazine Fuels and Their Selected Oxidation Products Using Differential Absorption Scattering Lidar[a]

Compound	$^{12}C^{16}O_2$ Laser Wavelength				$\sigma_r(\lambda_r)$ (cm^{-1} atm^{-1})	$\sigma_{nr}(\lambda_{nr})$[b] ($cm^{-1}$ atm^{-1})	Estimated Minimum Detectable Concentration, n_{min}[c] (atm)
	λ_r(μm)	Transition	λ_{nr}(μm)	Transition			
Hydrazine	10.441	P(4)	10.494	P(10)	7.56	2.82	5.3×10^{-8}
	10.718	P(32)	10.674	P(28)	6.18	2.17	6.2×10^{-8}
	10.810	P(40)	10.858	P(44)	7.45	2.81	2.2×10^{-8}
Monomethylhydrazine	10.334	R(8)	10.303	R(12)	3.48	0.78	9.3×10^{-8}
	10.883	P(46)	10.696	P(30)	2.06	1.01	2.4×10^{-7}
Unsymmetrical Dimethylhydrazine	10.834	P(42)	10.453	P(6)	3.95	0.05	6.4×10^{-8}
	10.858	P(44)	10.453	P(6)	3.95	0.05	6.4×10^{-8}
Ammonia	9.219	R(30)	9.260	R(22)	56.2	0.0489	4.5×10^{-9}
	10.349	R(6)	10.170	R(32)	26.3	0.010	9.5×10^{-9}
Monomethylamine[d]	9.458	P(8)	9.536	P(18)	0.731	0.220	4.9×10^{-7}
	9.586	P(24)	9.536	P(18)	0.881	0.220	3.8×10^{-7}
	9.714	P(38)	9.536	P(18)	0.748	0.220	4.7×10^{-7}
Dimethylamine	9.621	P(28)	9.443	P(6)	0.80	0.18	4.0×10^{-7}
Trimethylamine	9.586	P(24)	9.774	P(44)	4.15	1.72	1.0×10^{-7}
Methanol	9.443	P(6)	9.621	P(28)	8.59	1.45	3.5×10^{-8}
	9.504	P(14)	9.621	P(28)	9.75	1.45	3.0×10^{-8}
	9.676	P(34)	9.621	P(28)	21.77	1.45	1.2×10^{-8}

[a] $^{12}C^{16}O_2$ laser-based lidar assumed.

[b] Uncertainties for absorption cross-section data given in Table I.

[c] Assumes a δ value of 0.5% and a range cell path length of 100 m [see Eq. (5)].

[d] Absorption caused by suspected ammonia impurities in methylamine spectrum in Fig. 12 is not considered.

B. ESTIMATES OF THE HYDRAZINE-FUEL DETECTABILITIES IN THE PRESENCE OF POSSIBLE ATMOSPHERIC INTERFERENCES

The absorption cross-section measurements presented in Section IV for the hydrazines and their selected degradation products are the basis information needed for the ambient air monitoring of these compounds. If the number of $^{12}C^{16}O_2$ laser lines m used to analyze an air sample is equal to or greater than the n absorbing components in the sample (whose $^{12}C^{16}O_2$ laser absorption cross sections are known), the unknown concentrations of each of the n components in a sample can be determined with the proper selection of laser lines. The accuracy of the concentrations of the n components determined in an ambient air sample depends upon: (1) the accuracy of the absorbance measurements made by the detection instrumentation, (2) the accuracy of the basis absorption cross-section data for each $^{12}C^{16}O_2$ laser absorbing component in the mixture, and (3) the choice and number of wavelengths used for monitoring. As presented in the appendix, the methods of matrix algebra are generally required to estimate the concentrations of each species in a multicomponent mixture and to select the optimum wavelengths for a fixed number of laser lines. The best $^{12}C^{16}O_2$ laser wavelengths for detection of a single species in the presence of interferences can usually be selected by visual comparison of the corresponding $^{12}C^{16}O_2$ laser absorption profiles. This procedure was used for the following discussion of the expected detectabilities of: (1) hydrazines and their selected oxidation products individually in the presence of typical ambient levels of water vapor, (2) hydrazines in the presence of water vapor and the selected air oxidation products of the hydrazines, and (3) hydrazines in the presence of water vapor and typical concentrations of pollutants found in urban air.

1. EFFECT OF WATER VAPOR ABSORPTION INTERFERENCE ON DETECTABILITIES OF HYDRAZINE FUELS AND THEIR SELECTED DEGRADATION PRODUCTS

The absorption cross sections for the water vapor absorption bands within the $^{12}C^{16}O_2$ laser region are very small, $\sim 10^{-4}$ cm^{-1} atm^{-1}.

However, the high relative concentration of water vapor in the ambient air causes background interference absorption that can set a lower sensitivity limit for the detection of various airborne species by $^{12}C^{16}O_2$ laser techniques. Figure 17 presents $^{12}C^{16}O_2$ laser absorption spectra of water vapor at pressures of 15 and 6.9 Torr. These spectra consist of a few absorption peaks on a broad continuum absorption background. At a water vapor pressure of 15 Torr, i.e., at about 50% RH at 29°C, water vapor absorption strengths of approximately 10^{-6} cm^{-1} are obtained throughout the $^{12}C^{16}O_2$ laser wavelength region.[36]

Because of the generally continuous nature of the water-vapor-absorption profile in this region, it is expected that maxima in the highly characteristic absorption profiles of Figs. 8 through 15 for the hydrazine fuels and their selected degradation products would be detectable at absorption strengths of $10^{-7}cm^{-1}$ or less using the $^{12}C^{16}O_2$ laser photoacoustic technique.* Thus, at a water vapor pressure of 15 Torr, the α_{min} value in Eq. (3) would increase to $10^{-7}cm^{-1}$, and the photoacoustic detection limits of the compounds listed in Table II would increase by about a factor of 100 from the 1-W laser power values indicated. In the presence of 15-Torr water vapor, the otherwise interference-free photoacoustic detection limit for hydrazine at either the P4 or P40 lines in the 10.4-μm $^{12}C^{16}O_2$ laser band becomes 13 ppb. The corresponding detection limit for MMH becomes 29 ppb at the 10.4-μm band R8 line, while that for UDMH becomes approximately

*The absorption profiles of these species are expected to be recognizable for absorption signals that are 10% of the water background absorption. Improvements in this 10^{-7} cm^{-1} detection sensitivity assumed above may be possible using Stark modulation spectroscopy to discriminate against water vapor continuum absorption. This method is based on the fact that molecules with dipole moments can have their energy levels shifted by application of an electric field. Thus, a modulated electric field may be used to shift the absorption lines of such molecules into and out of resonance with a given laser wavelength. The resulting modulated absorption signal of the species of interest can be amplified relative to that of the water continuum absorption. The latter absorption signal remains unmodulated by the time-varying electric field.

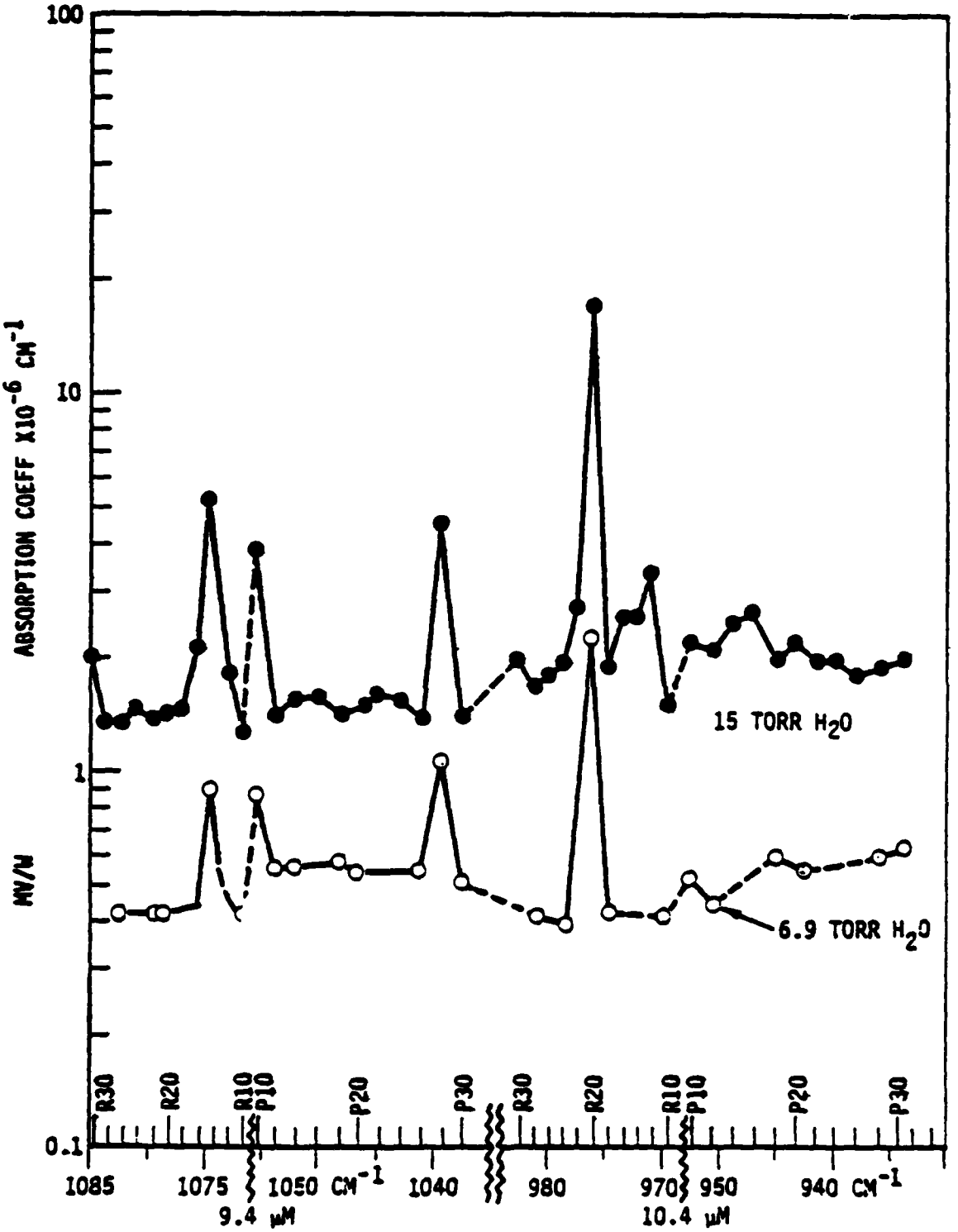

Fig. 17. $^{12}C^{16}O_2$ Laser Absorption Spectra of Water Vapor (from Ref. 36)

25 ppb for the P40 through P44 lines of the 10.4-μm band. These estimated detection limits are below the lowest proposed threshold limit values for the hydrazines (see Section I). The detection limits for other compounds listed in Table II in the presence of 15 Torr water vapor, but otherwise detected alone, would be as follows: ammonia (2 ppb at the $^{12}C^{16}O_2$ laser 9.4-μm band R30 line), methylamine (110 ppb at the 9.4-μm P24 line), dimethylamine (120 ppb at the 9.4-μm P42 line), trimethylamine (24 ppb at the 9.4-μm P24 line), and methanol (4.6 ppb at the 9.4-μm P34 line).

The presence of water vapor in the ambient air samples monitored by the $^{12}C^{16}O_2$ laser long-path absorption technique is not expected to significantly increase the interference-free detectabilities listed in Table III for the hydrazines and their oxidation products. In fact, Steinfeld and Green[37] demonstrated that the presence of a broadly absorbing "interference" gas may actually decrease the long-path absorption detection limit of a low concentration species in a mixture when the absorption of the laser light by the mixture is small, and the individual absorbances of the various species in the mixture are uncertain because of baseline fluctuations. The addition of a broadly absorbing gas decreases the effect of the fluctuations by increasing the total absorbance of the sample. The larger total absorbance results in more sensitive measurements.

The differential absorption scattering lidar technique would be immune from interferences with equal absorption coefficients at the two wavelengths λ_r and λ_{nr} used for monitoring a given species, because the technique measures a power ratio to yield the total $\Delta\alpha$ in the range cell. As a result, species for which $\Delta\alpha = 0$ do not represent interferences. The generally continuous absorption background of water vapor in the $^{12}C^{16}O_2$ laser region offers the possibility of selecting λ_r and λ_{nr} wavelengths to detect the hydrazines or degradation products of the hydrazines while discriminating against water. The interference-free detection limits listed for the compounds in Table IV for the $^{12}C^{16}O_2$ laser-based lidar technique are thus not expected to increase significantly in the presence of water vapor.

2. DETECTABILITIES OF THE HYDRAZINES IN THE PRESENCE OF WATER VAPOR AND SELECTED AIR OXIDATION PRODUCTS OF THE HYDRAZINES

Hydrazine, MMH, and UDMH are observed in Figs. 8 through 10 to exhibit their strongest absorbances within the $^{12}C^{16}O_2$ laser 10.4-μm bands. However, small or nearly zero absorbances are observed in Figs. 12 through 15 within the 10.4-μm band of the $^{12}C^{16}O_2$ laser for methylamine (when the suspected ammonia impurity peaks are ignored), dimethylamine, trimethylamine, and methanol. Ammonia is observed in Fig. 11 to possess sharp absorption features within the $^{12}C^{16}O_2$ laser 10.4-μm band at the R8, R6, and R4 lines, as well as at the P34 and P32 lines. Because these absorption features are easily recognizable, it should not be difficult to separate the contribution of ammonia to the total absorption. The absorption cross sections for ammonia at most of the $^{12}C^{16}O_2$ laser lines within the 10.4-μm band are less than 0.8 $cm^{-1}atm^{-1}$. The absorption cross sections for methylamine, dimethylamine, trimethylamine, and methanol are less than 0.1 $cm^{-1}atm^{-1}$, 0.4 $cm^{-1}atm^{-1}$, 0.1 $cm^{-1}atm^{-1}$, and ~0.2 $cm^{-1}atm^{-1}$, respectively, throughout much of the $^{12}C^{16}O_2$ laser 10.4-μm region. It is expected that a species would require an absorbance of approximately 10^{-7} cm^{-1}, i.e., 10% of the water background absorption, before it would constitute an important interference to the detection of the hydrazines at the 30-ppb level. Absorbing interferences of this size would correspond to concentrations of roughly 130 ppb for ammonia, 1 ppm for methylamine, 250 ppb of dimethylamine, 1 ppm for trimethylamine, and 500 ppb for methanol. The concentrations of ammonia, methylamine, dimethylamine, trimethylamine, and methanol in typically polluted urban air are well below these levels. It is highly unlikely that the airborne concentrations of these compounds could ever reach the foregoing levels as the result of atmospheric degradation reactions of the hydrazines unless the hydrazines were present at levels well above 30 ppb. It is not expected that the detection limits estimated in the previous subsection for the hydrazines in the presence of water vapor alone will be significantly increased by the presence of the hydrazine oxidation products.

3. DETECTION OF HYDRAZINES IN THE PRESENCE OF WATER VAPOR AND TYPICAL POLLUTANTS FOUND IN THE URBAN AIR

The detection limits of selected compounds in a multicomponent mixture by $^{12}C^{16}O_2$ laser spectroscopic techniques generally increase from their interference-free values with: (1) the increasing number of $^{12}C^{16}O_2$ laser absorbing interferences, (2) the increasing absorptivities of these interferences, and (3) the greater degree of spectral similarity between the compounds of interest and the interferences. This subsection describes the interferences expected at different detection locations for the hydrazine fuels and their toxic degradation products. Where available, vapor-phase infrared absorption data for the $^{12}C^{16}O_2$ laser region are presented for these potential interferences.

The types and concentrations of potential interferences to the detection of the hydrazines or their toxic degradation products by $^{12}C^{16}O_2$ laser spectroscopic techniques will vary with the detection location. Generally, the potential interferences of highest concentration are expected to be those pollutants in urban air that result primarily from auto emissions. Additional interferences may become important if detection is to be carried out near hydrazine-fuel production sites in major chemical industry centers. In this case, the most important interferences may be chlorinated and fluorinated compounds used as commerical solvents or propellants, and compounds associated with plastics and/or rubber industrial use, e.g., the acrylates and methacrylates, styrene, and butadiene and its derivatives. The concentrations of pollutants typically found at non-urban Air Force installations are expected to be low compared with those found in urban and industrial locations. However, other interferences associated with certain Air Force operations may be present, including constituents and combustion products of jet fuel, degreasing solvents, and the volatile constituents of paints and corrosion inhibitors.

Table V lists the typical concentrations of various pollutants in urban air along with their corresponding infrared absorption properties within the wavelength regions of $^{12}C^{16}O_2$ laser output. Where available, $^{12}C^{16}O_2$

laser absorption spectral data are presented; otherwise, low-resolution absorption data from standard reference spectra are given.

Of the inorganic compounds CO, NO, NO_2, N_2O, O_3, NH_3, and SO_2 listed in Table V, only the last three possess absorption within the wavelength intervals of $^{12}C^{16}O_2$ laser output. As discussed in the previous subsection, ammonia (NH_3) (at the 2 to 20 ppb concentration range typically found in urban air[24]) is not expected to severely interfere with the detection of the hydrazines. Sulfur dioxide (SO_2) absorbs weakly in the $^{12}C^{16}O_2$ laser 9.4-μm band R branch and exhibits practically no absorption in the rest of the $^{12}C^{16}O_2$ laser region.[28] Ozone (O_3) possesses strong absorption features within the $^{12}C^{16}O_2$ laser 9.4-μm band P branch but absorbs only weakly within the 9.4-μm band R branch and throughout the 10.4-μm band.[25,26] Neither ozone nor sulfur dioxide would thus be expected to significantly increase the $^{12}C^{16}O_2$ laser spectroscopic detection limits estimated earlier for the hydrazines in the presence of water vapor only, since the strongest $^{12}C^{16}O_2$ laser absorbances for the hydrazines fall within the 10.4-μm laser band.

More than 50 different hydrocarbons have been found in typically polluted urban air samples.[45,46] The average concentrations of the most abundant hydrocarbons found in a series of 200 samples of air taken in the Los Angeles area during 1965 were as follows:[45,46] methane (3.22 ppm), ethane (0.10 ppm), propane (0.05 ppm), n-butane (0.06 ppm), n-pentane (0.03 ppm), i-pentane (0.04 ppm), ethylene (0.06 ppm), benzene (0.03 ppm), and toluene (0.05 ppm). The highest concentrations listed in Table V for some of these same compounds[42] tend to be lower than the average concentrations found in the 1965 Los Angeles study.[45,46] The concentration ranges in Table V for n-butane, the pentanes, benzene, and toluene were obtained for air samples taken in downtown Berlin, Germany during 1978.[42] The saturated hydrocarbons methane, ethane, and propane exhibit negligible absorption[47] within the $^{12}C^{16}O_2$ laser 9.4-μm bands and will not interfere with the detection of the hydrazines. The compounds: n-butane,[25]

Table V. Typical Concentrations of Pollutants in Urban Air and Their Corresponding Absorption Properties in the $^{12}C^{16}O_2$ Laser Region

Pollutants	Concentration Range (ppb)	Ref.	Resolution	9.4μm Band: 1069-1089 cm^{-1}	9.4μm Band: 1023-1059 cm^{-1}	10.4μm Band: 965-989 cm^{-1}	10.4μm Band: 919-958 cm^{-1}	Ref.
CO	2000-20,000	38	$2cm^{-1}$	No abs.	No abs.	No abs.	No abs.	43
NO	10-150	38	$2cm^{-1}$	No abs.	No abs.	No abs.	No abs.	44
NO_2	50-200	38	$2cm^{-1}$	No abs.	No abs.	No abs.	No abs.	44
N_2O	296;331	39; 40	$2cm^{-1}$	No abs.	No abs.	No abs.	No abs.	44
O_3	20-200	38	CO_2 laser	—	$\sigma(\lambda)>12.0 cm^{-1}atm^{-1}$ at P(8), P(12), P(14) all other $\sigma(\lambda)<9.5 cm^{-1}atm^{-1}$	—	—	26 (See also 25)
Totally saturated hydrocarbons other than CH_4	200-500	38	—	—	—	—	—	
Alkenes	20-60	38	CO_2 laser	C_2H_4: a $\sigma(\lambda)<2.2 cm^{-1}atm^{-1}$	C_2H_4: all $\sigma(\lambda)<0.65 cm^{-1}atm^{-1}$	C_2H_4: all $\sigma(\lambda)\leq 5.0 cm^{-1}atm^{-1}$	C_2H_4: $\sigma(\lambda)=29.1 cm^{-1}atm^{-1}$ P(14). All other $\sigma(\lambda)$ $<5.0 cm^{-1}atm^{-1}$	26 (See also 25)
Aromatics	100-300	38						
Aldehydes	50-250	38	$2 cm^{-1}$	propanal: $\gamma(\lambda)_{max}\approx 1.03 cm^{-1}atm^{-1}$	propanal: $\sigma(\lambda)_{max}\approx 0.13 cm^{-1}atm^{-1}$	propanal: $\sigma(\lambda)_{max}\approx 0.04 cm^{-1}atm^{-1}$	propanal: $\sigma(\lambda)_{max}\approx 0.40 cm^{-1}atm^{-1}$	47
PAN	10-40	38						
NH_3	2-20	24	CO_2 laser	$\sigma(\lambda)=56.2 cm^{-1}atm^{-1}$ at R(30) $=11.2$ " " at R(16) all other $\sigma(\lambda)\leq 1.7 cm^{-1}atm^{-1}$	all $\sigma(\lambda)<3.8 cm^{-1}atm^{-1}$	$\sigma(\lambda)>10.0 cm^{-1}atm^{-1}$ at R(4)-R(8). All other $\sigma(\lambda)<6.5 cm^{-1}atm^{-1}$	$\sigma(\lambda)>10.0 cm^{-1}atm^{-1}$ at P(32), P(34). All other $\sigma(\lambda)<8.5 cm^{-1}atm^{-1}$	24
SO_2	2000	41	CO_2 laser	all $\sigma(\lambda)\leq 0.11 cm^{-1}atm^{-1}$	all $\sigma(\lambda)\leq 0.01 cm^{-1}atm^{-1}$	all $\sigma(\lambda)\leq 0.005 cm^{-1}atm^{-1}$	all $\sigma(\lambda)\leq 0.005 cm^{-1}atm^{-1}$	27
n-butane	5-22	42	CO_2 laser	all $\sigma(\lambda)\leq 0.02 cm^{-1}atm^{-1}$	all $\sigma(\lambda)\leq 0.03 cm^{-1}atm^{-1}$	all $\sigma(\lambda)\leq 0.6 cm^{-1}atm^{-1}$	all $\sigma(\lambda)\leq 0.61 cm^{-1}atm^{-1}$	25
i-pentane	4-34	42	$2 cm^{-1}$	Negligible abs.	$\sigma(\lambda)_{max}\approx 0.25 cm^{-1}atm^{-1}$	$\sigma(\lambda)_{max}\approx 0.28 cm^{-1}atm^{-1}$	$\sigma(\lambda)_{max}\approx 0.10 cm^{-1}atm^{-1}$	48
n-pentane	3-26	42	$2 cm^{-1}$	$\sigma(\lambda)max\approx 0.069 cm^{-1}atm^{-1}$	$\gamma(\lambda)_{max}\approx 0.093 cm^{-1}atm^{-1}$	$\sigma(\lambda)_{max}\approx 0.048 cm^{-1}atm^{-1}$	$\sigma(\lambda)_{max}\approx 0.27 cm^{-1}atm^{-1}$	48
cyclohexane	—	—	CO_2 laser	all $\sigma(\lambda)<0.01 cm^{-1}atm^{-1}$	all $\sigma(\lambda)<0.3 cm^{-1}atm^{-1}$	all $\sigma(\lambda)<0.01 cm^{-1}atm^{-1}$	all $\sigma(\lambda)\leq 0.02 cm^{-1}atm^{-1}$	34
benzene	5-31	42	CO_2 laser	all $\sigma(\lambda)\leq 0.05 cm^{-1}atm^{-1}$	all $\sigma(\lambda)\leq 2.0 cm^{-1}atm^{-1}$	all $\sigma(\lambda)<0.05 cm^{-1}atm^{-1}$	$\sigma(\lambda)<0.05 cm^{-1}atm^{-1}$	27
toluene	4-41	42	$2cm^{-1}$	$\gamma(\lambda)_{max}\approx 2.9\pm 1.0 cm^{-1}atm^{-1}$	$\sigma(\lambda)max\approx 1.6 cm^{-1}atm^{-1}$	Negligible abs.	Negligible abs.	43
m-/p-xylenes	6-18	42	$2cm^{-1}$	p-xylene: $\sigma(\lambda)_{max}\approx 0.40 cm^{-1}atm^{-1}$	p-xylene $\sigma(\lambda)_{max}\approx 0.59 cm^{-1}atm^{-1}$	p-xylene Negligible abs.	p-xylene: Negligible abs.	43
Freon 11 CCl_3F	0.10;0.13	39; 40	CO_2 laser	$\sigma(\lambda)>20 cm^{-1}atm^{-1}$ at R(18)-R(20) $\sigma(\lambda)<20 cm^{-1}atm^{-1}$ at R(8) - R(16)	all $\sigma(\lambda)<0.10 cm^{-1}atm^{-1}$	all $\sigma(\lambda)<0.10 cm^{-1}atm^{-1}$	$\sigma(\lambda)>2.0 cm^{-1}atm^{-1}$ at P(86)-P(36) $\sigma(\lambda)<2.0 cm^{-1}atm^{-1}$ at P(6) - P(24)	27 (See also 25)
Freon 12 CCl_2F_2	0.18;0.23	39; 40	CO_2 laser	$\gamma(\lambda)>10 cm^{-1}atm^{-1}$ at R(26)-R(28) all other $\sigma(\lambda)<10 cm^{-1}atm^{-1}$	all $\sigma(\lambda)<0.10 cm^{-1}atm^{-1}$	all $\sigma(\lambda)<0.10 cm^{-1}atm^{-1}$	$\sigma(\lambda)>10 cm^{-1}atm^{-1}$ at P(30)-P(38) $\sigma(\lambda)<10 cm^{-1}atm^{-1}$ at P(6)-P(28)	27 (See also 25)
Freon 113 $C_2Cl_3F_3$	0.016;0.021	39; 40	CO_2 laser	all $\sigma(\lambda)<1.1 cm^{-1}atm^{-1}$	$\sigma(\lambda)>10.0 cm^{-1}atm^{-1}$ at P(16)-P(20) P(24) P(26) all other $(\lambda)<10.0 cm^{-1}atm^{-1}$	all $\sigma(\lambda)<0.58 cm^{-1}atm^{-1}$	all $\sigma(\lambda)<6.7 cm^{-1}atm^{-1}$	34
Freon 114 $C_2Cl_2F_4$	0.009	40	CO_2 laser	all $\sigma(\lambda)<1.0 cm^{-1}atm^{-1}$	$\sigma(\lambda)\geq 10 cm^{-1}atm^{-1}$ at P(8)-P(32) $\sigma(\lambda)<10 cm^{-1}atm^{-1}$ at P(34)	all $\sigma(\lambda)<0.56 cm^{-1}atm^{-1}$	$\sigma(\lambda)\geq 10.0 cm^{-1}atm^{-1}$ at P(36)-P(40) $\sigma(\lambda)<10.0 cm^{-1}atm^{-1}$ at P(4)-P(34)	25
CCl_4	0.11;0.12	39; 40	$2cm^{-1}$	No abs.	No abs.	No abs.	No abs.	43
CH_3Cl	0.95;0.57	39; 40	$2cm^{-1}$	$\sigma(\lambda)_{max}\approx 1.0 cm^{-1}atm^{-1}$	$\sigma(\lambda)_{max}\approx 0.38 cm^{-1}atm^{-1}$	$\sigma(\lambda)_{max}\approx 0.18 cm^{-1}atm^{-1}$	Negligible abs.	43
CH_3CCl_3	0.084;0.095	39; 40	CO_2 laser	$\sigma(\lambda)_{max} = 9.93 cm^{-1}atm^{-1}$	$\gamma(\lambda)_{max} = 0.93 cm^{-1}atm^{-1}$	$\sigma(\lambda)_{max} = 0.07 cm^{-1}atm^{-1}$	$\sigma(\lambda)_{max} = 0.07 cm^{-1}atm^{-1}$	34

n-pentane,[48] and i-pentane[48] possess absorption bands of 0.6 cm^{-1} atm^{-1}, 0.3 cm^{-1} atm^{-1}, and 0.3 cm^{-1} atm^{-1}, respectively, or less within the $^{12}C^{16}O_2$ laser 10.4-μm band. At the levels found in the 1965 Los Angeles study,[45,46] n-pentane and i-pentane should negligibly increase, while n-butane should only slightly increase the estimated detection limits for the hydrazines in the presence of ambient levels of water vapor.

Like ammonia, ethylene[26] (C_2H_4) exhibits a highly characteristic and easily recognizable $^{12}C^{16}O_2$ laser absorption profile. Ethylene possesses a single strong absorption feature with a cross section of 29.1 cm^{-1} atm^{-1} at the P14 line of the $^{12}C^{16}O_2$ laser 10.4-μm band.[26] This strong ethylene absorption feature does not coincide with the strongest absorption features of hydrazine, MMH, or UDMH. The $^{12}C^{16}O_2$ laser 10.4-μm band wavelengths available where the ethylene absorption cross sections are low* may be well-suited for monitoring the hydrazines. These 10.4-μm band laser lines and their corresponding ethylene absorption cross sections are: R32(0.83 cm^{-1} atm^{-1}), R30(0.56 cm^{-1} atm^{-1}), R8(0.99 cm^{-1} atm^{-1}), P22(1.09 cm^{-1} atm^{-1}), P28(1.30 cm^{-1} atm^{-1}), P30 (1.63 cm^{-1} atm^{-1}), P32(0.48 cm^{-1} atm^{-1}), and P34(0.54 cm^{-1} atm^{-1}).[26] It is apparent that ethylene concentrations of about 100 ppb at these wavelengths would produce absorbances of 10^{-7} cm^{-1}. For ethylene concentrations below 100 ppb, the $^{12}C^{16}O_2$ laser detection limits should not significantly increase over those estimated in the presence of 15 Torr water vapor and no other interferences. The average ethylene concentration found in the 1965 Los Angeles study was 60 ppb.[45,46]

The aromatic hydrocarbons benzene,[27] toluene,[43] and p-xylene[43] all absorb negligibly in the $^{12}C^{16}O_2$ laser 10.4-μm band and should not interfere

*Ethylene $^{12}C^{16}O_2$ laser absorption data were reported by Patty et al.[26] and Mayer et al.[27] As found for their ammonia data, it appears that the ethylene absorption data have been mislabelled according to laser line transitions by Mayer et al. in the $^{12}C^{16}O_2$ laser 9.4-μm band P branch. Differences of about a factor of 2 in the absorption cross sections can also be observed for ethylene at certain lines within the $^{12}C^{16}O_2$ laser 10.4-μm band between the two sets of data. The data of Patty et al.[26] are used here. Their ethylene measurements were limited to the R32 to R8 and the P10 to P34 lines of the $^{12}C^{16}O_2$ laser 10.4-μm band.[26]

with detection of the hydrazines. The chlorofluorocarbons in Table V, CCl_3F,[25,27] CCl_2F_2,[25,27] $C_2Cl_3F_3$,[34] and $C_2Cl_2F_4$,[25] all possess moderate absorption bands within the $^{12}C^{16}O_2$ laser 10.4-μm band P branch where the hydrazines absorb. However, the background levels of these compounds in the ambient air are quite low,[39,40] so these compounds should not interfere with detection of the hydrazines by $^{12}C^{16}O_2$ laser techniques.

Data were obtained in previous studies to characterize the organic vapors present in the ambient air of airport baggage make-up areas.[49] These data are relevant to the special case of monitoring for the hydrazines and their degradation products where jet fuel is used. The previous studies[49] were carried out to determine potential interferences to the detection of volatile vapors from clandestine explosive devices in airport terminals. The largest concentrations of organic vapors (all less than 50 ppb by volume) were found for acetone, propanal, furan, benzene, toluene, the xylenes, the trimethylbenzenes, and styrene. Several of these molecules exhibit absorbances within the wavelength regions of $^{12}C^{16}O_2$ laser output.* Benzene, toluene and p-xylene absorb weakly within the $^{12}C^{16}O_2$ laser 10.4-μm band and should not interfere with detection of the hydrazines.

*Except for those molecules previously discussed and propanal, the absorption properties of these compounds are not listed in Table V. The approximate positions of the absorption band centers, within the general wavelength region of $^{12}C^{16}O_2$ laser output, and absorption intensities (relative to the strongest band at each molecule) in the vapor phase for some of these possible interferences are:[43] acetone, 9.17 μm(w); 11.11 μm(w) propanal, 9.09 μm(w-m); benzene, 9.62 μm(m); toluene, 9.09 μm(m); 1,2-dimethylbenzene, 9.47 μm, 9.76 μm, 10.15 μm(w); 1,4-dimethylbenzene, 9.52 μm, 9.71 μm(w); 1,2,4-trimethylbenzene, 9.97 μm(w), 10.08 μm(s); and styrene, 10.99 μm(s), 9.17 μm, 9.26 μm, 9.80 μm(w). Here s, m, and w denote strong, moderate, and weak band intensities, respectively. For molecules for which vapor phase data are unavailable, the corresponding neat liquid phase data are: furan, 9.42 μm(w-m), 10.10 μm(s); 1,2,3-trimethylbenzene, 9.18 μm(m), 9.94 μm(w-m), 10.18 μm(w); and 1,3,5-trimethylbenzene, 9.68 μm(w).[50]

Based on low resolution (~2 cm^{-1}) vapor phase absorption spectra, acetone, propanal, and styrene possess absorption bands with cross sections of 1.30 cm^{-1} atm^{-1}, 0.40 cm^{-1} atm^{-1}, and 2.6 cm^{-1} atm^{-1}, respectively, or less within the $^{12}C^{16}O_2$ laser 10.4-μm band. Therefore, acetone, propanal, and styrene concentrations below approximately 75, 250, and 40 ppb, respectively, should not significantly increase the detection limits estimated for the hydrazines in the presence of 15 Torr water vapor. However, $^{12}C^{16}O_2$ laser vapor-phase absorption spectra will be required for these compounds as well as for furan, the xylenes (other than p-xylene), and the trimethylbenzenes to thoroughly assess their effect on the detectabilities of the hydrazines by $^{12}C^{16}O_2$ laser spectroscopic methods.

It may be of interest to detect hydrazine and UDMH in the presence of one another, since a 1:1 mixture of each (Aerozine 50) is extensively used as a rocket propellant. Figure 8 indicates that hydrazine exhibits an absorption profile of a series of sharp peaks and valleys throughout both the R and P branches of the $^{12}C^{16}O_2$ laser of 10.4-μm band. However, UDMH in Fig. 10 exhibits negligible absorption within the R branch and between lines P4 and about P20 of the $^{12}C^{16}O_2$ laser 10.4-μm band. It should be possible to readily detect hydrazine in the presence of UDMH by monitoring hydrazine absorption at any of its strong absorption features throughout the $^{12}C^{16}O_2$ laser 10.4-μm band R branch and lines P4 to P20 of the P branch. UDMH should also be detectable in the presence of hydrazine by monitoring UDMH absorption in the hydrazine absorption valleys at the $^{12}C^{16}O_2$ laser 10.4-μm band lines P28 and P30, P36 and P38, and P44 and P46.

It is also expected that it will be necessary to monitor airborne levels of the hydrazines at locations where the rocket fuel oxidizing agent N_2O_4 is in extensive use. Neither N_2O_4 itself[44] nor any of its expected major atmospheric degradation products (NO,[44] NO_2,[44] N_2O_5,[44] HNO_3,[51] HONO[52]) exhibits absorption bands within the $^{12}C^{16}O_2$ laser region that would increase the detection limits of the hydrazines by $^{12}C^{16}O_2$ laser spectroscopic techniques.

VI. CONCLUSIONS

The threshold limit values adopted by ACGIH for human exposure to hydrazine, MMH, and UDMH in the ambient air of 100, 200, and 500 ppb, respectively, are much less stringent than the corresponding values of 30, 40, and 60 ppb recently recommended to OSHA by NIOSH. OSHA is expected to adopt one of these sets of thresholds as their new allowable exposure standard for the hydrazines.

In Section V it was estimated that 30-ppb detection sensitivities or less should be obtainable by the $^{12}C^{16}O_2$ laser photoacoustic technique for each of the hydrazines in the presence of 15 Torr water vapor. Long-path absorption detection sensitivities of 70, 140, and 130 ppb were estimated for hydrazine, MMH, and UDMH, respectively, under the same conditions with the use of a 100-m path length absorption cell. The corresponding lidar detection sensitivities for these compounds in the presence of 15 Torr of water vapor were estimated to be 50, 90, and 60 ppb using a lidar range cell path length of 100 m.

Analysis of the typical concentrations of the pollutants normally found in the urban air and their infrared spectral properties indicated that the $^{12}C^{16}O_2$ laser spectroscopic detection sensitivities of the hydrazines should not be significantly increased over the foregoing estimates by these pollutants. It was also concluded that the concentrations of the compounds ammonia, methylamine, dimethylamine, trimethylamine, and methanol resulting from atmospheric degradation reactions of the hydrazines would be too low to interfere with detection of the hydrazines. In certain industrial locations, the concentrations of selected $^{12}C^{16}O_2$ laser absorbing species may be large enough to increase the detection limits of the hydrazines. To obtain accurate hydrazine concentrations in these cases, simultaneous equation solution methods as outlined in the appendix will be required. Such situations will require a library of $^{12}C^{16}O_2$ laser absorption cross-section data for each interfering species. Industrial chemicals for which such data

may be required include various chlorofluorocarbons and various monomer species associated with the plastics industry.

It is concluded that the $^{12}C^{16}O_2$ laser-based photoacoustic, long-path absorption, and lidar detection methods would all provide the sensitivities required for real-time detection of the hydrazines at the threshold levels adapted by ACGIH. However, only the $^{12}C^{16}O_2$ laser-based photoacoustic technique will provide the sensitivities necessary for real-time detection of hydrazines at the NIOSH-recommended threshold levels. Hydrazine detection by the $^{12}C^{16}O_2$ laser photoacoustic technique may be possible down to the level of a few parts per billion if the water vapor continuum background absorption can be discriminated against by techniques such as Stark modulation spectroscopy. Work is now in progress to establish detection limits for the hydrazines with the use of a laboratory $^{12}C^{16}O_2$ laser photoacoustic detection system.

APPENDIX

METHODS TO ESTIMATE THE CONCENTRATIONS OF SPECIES IN A MULTICOMPONENT MIXTURE

The expected absorbance y_i of an n-component sample at wavelength i is given by the expression

$$y_i = \ell \sum_{j=1}^{n} \sigma_{ij} p_j \qquad i = 1, \ldots\ldots, m \tag{A1}$$

Here, ℓ is in the path length of light absorbed, σ_{ij} is the absorption cross section of the j-th component in the mixture at wavelength i, and p_j is the partial pressure of the j-th component in the mixture. When the number of laser wavelengths m is equal to or greater than the number of $^{12}C^{16}O_2$ laser absorbing species n, the unknown partial pressures of each of the n components in the mixture p_j can be, in principle, calculated from the measured absorbance A_i. This requires knowledge of the path length ℓ and the absorption cross sections σ_{ij} of the n components in the mixture over at least n of the m wavelengths.

One method of estimating the p_j values is with the aid of the inverse of the matrix σ_{ij}

$$p_j = \frac{1}{\ell} \sum_{j=1}^{n} \sigma_{ji}^{-1} y_i \approx \frac{1}{\ell} \sum_{i=1}^{n} \sigma_{ji}^{-1} A_i \tag{A2}$$

The approximately equal sign in Eq. (A2) refers to the fact that the measured absorbances A_i and the expected absorbances y_i are not necessarily equal. The precision with which Eq. (A2) can be solved depends on the properties of the inverse matrix σ_{ji}^{-1} and the precision with which the A_i can be measured.[18b] The most precise values of p_j result when the laser wavelengths are chosen such that σ_{ji}^{-1} is diagonalized as well as possible, i.e., the wavelengths are selected to minimize interference among the n components in the mixture.

Steinfeld and Green[34,37] found that small measurement errors in the A_i can lead to large uncertainties in the p_j values when matrix inversion methods are used directly. As a result, they used a procedure to least-squares fit the absorption data to remove experimental fluctuations prior to solution for the pressure values p_j. For these analyses, Steinfeld and Green used a larger number of wavelengths m than components n in the mixture. By the least-squares fit procedure, the best set of solutions for the pressures p_j of the species in a multicomponent mixture are obtained when the differences between y_i and A_i are smallest. This occurs when

$$\frac{\partial\left[\sum_{j=1}^{n}(\sigma_{ij}p_j\ell - A_i)^2\right]}{\partial p_j} = 0 \quad \begin{matrix} i = 1,\ldots.. m \\ j = 1,\ldots.. n \end{matrix} \tag{A3}$$

Solving Eq. (A3) results in a set of m simultaneous equations:

$$\begin{matrix} (\sigma_{11}^2 + \sigma_{11}\sigma_{12} + \cdots \sigma_{11}\sigma_{1n})\,p_1 + (\sigma_{12}^2 + \sigma_{11}\sigma_{12} + \cdots \sigma_{12}\sigma_{1n})\,p_2 + \cdots (\sigma_{1n}^2 + \sigma_{11}\sigma_{1n} + \cdots \sigma_{1,n-1}\sigma_{1n})\,p_n = (\sigma_{11} + \cdots \sigma_{1n})A_1/\ell \\ \vdots \qquad\qquad\qquad\qquad\qquad\qquad\qquad\qquad\qquad\qquad\qquad\qquad\qquad\qquad\qquad\qquad \vdots \\ (\sigma_{m1}^2 + \sigma_{m1}\sigma_{m2} + \cdots \sigma_{m1}\sigma_{mn})\,p_1 + \cdots \qquad\qquad \cdots\cdots \qquad\qquad (\sigma_{mn}^2 + \sigma_{m1}\sigma_{mn} + \cdots \sigma_{m,n-1}\sigma_{mn})\,p_n = (\sigma_{m1} + \cdots \sigma_{mn})A_m/\ell \end{matrix} \tag{A4}$$

The m simultaneous equations can be compacted to a set of n simultaneous equations so all m of the wavelength measurements can be utilized.

$$f_{j1}p_1 + f_{j2}p_2 + \cdots f_{jn}p_n = \sum_{i=1}^{n}\sigma_{ij}A_i/\ell = d_j \tag{A5}$$

$$j = 1,\ldots n$$

where

$$f_{jk} = \sum_{i=1}^{n}\sigma_{ij}\sigma_{ik} \tag{A6}$$

This system of m equations can be solved by the use of the matrix equation

$$\begin{bmatrix} f_{11} & f_{12} \cdots\cdots\cdots & f_{1n} \\ \cdot & f_{22} & \cdot \\ \cdot & & \cdot \\ \cdot & & \cdot \\ \cdot & & \cdot \\ \cdot & & \cdot \\ f_{n1} & \cdots\cdots\cdots\cdots & f_{nn} \end{bmatrix} \begin{bmatrix} p_1 \\ \cdot \\ \cdot \\ \cdot \\ \cdot \\ \cdot \\ p_n \end{bmatrix} = \begin{bmatrix} d_1 \\ \cdot \\ \cdot \\ \cdot \\ \cdot \\ \cdot \\ d_n \end{bmatrix} \qquad \text{(A7)}$$

To solve Eq. (A7), Steinfeld and Green used a matrix decomposition method to break the matrix on the left into two triangular matrices which are transpositions of one another. This procedure minimized the rounding errors in the matrix elements calculated during matrix decomposition. The triangular decomposition procedure allowed the p_j values to be obtained by back-substitution. Much less mathematical instability was introduced into the solution process by this method than by matrix inversion techniques.

REFERENCES

1. R. Beck, W. Englisch, and K. Gurs, Table of Laser Lines in Gases and Vapors, 2nd ed., Springer Series in Optical Sciences, Vol. 2, (Springer-Verlag Berlin Heidelberg, New York, 1978).

2. J. N. Pitts, Jr., D. Grosejean, K. Van Cauwenberghe, J. P. Schmid, and D. R. Fitz, Environ. Sci. and Technol. 12, 946 (1977).

3. D. Shapley, Science, 191, 268 (1976).

4. Ronald C. Shank, Recent Advances in the Toxicology of N-Nitroso and Hydrazine Compounds, AMRL-TR-74-125 (December 1974).

5. NIOSH Registry of Toxic Effects of Chemical Substances, 1977 ed., Vol II, U.S. Dept. of Health, Education, and Welfare.

6. National Safety News, "Threshold Limit Values for Chemical Substances in Workroom Air," September 1977, pp 85-92, Adopted by ACGIH for 1977.

7. (a) Occupational Safety and Health Reporter, "NIOSH Recommendations for a Hydrazines Standard," by the Bureau of National Affairs, Inc. (October 19, 1978).

   (b) NIOSH Manual of Analytical Methods, 2nd ed., Vol I-III, U.S. Dept. of Health, Education and Welfare (1977).

8. L. J. Luskus, "The Monitoring of Hydrazine Fuels in Air by Chemiluminescence," presented at the Second Conference on Environmental Chemistry of Hydrazine, Tyndal AFB, Fla., 15 February 1979.

9. R. A. Saunders, J. J. De Corpo, B. J. Stammerjohn, and R. J. Kautter, Evaluation of an Electrochemical Detector for Trace Concentrations of Hydrazine Compounds in Air, Naval Research Laboratory, Washington, D.C., NRL Report 8199 (April 13, 1978).

10. Data Sheet UA-123, MDA Scientific, Inc., 808 Busse Hwy., Park Ridge, Ill. 60068.

11. M. H. Mach, A. M. Baumgartner, GC/GC-MS Analysis of UDMH Oxidation Products, The Aerospace Corporation, El Segundo, Calif. (in preparation).

12. G. L. Loper, "Gas Phase Kinetic Study of Air Oxidation of UDMH," Proceedings of the Conference on Environmental Chemistry of Hydrazine Fuels, Tyndall AFB, 13 September 1977, pp. 129-159.

13. D. H. Fine, F. Rufeh, D. Lieb, and D. P. Roundbehler, Anal. Chem. 47, 1188-1191 (1975).

14. D. H. Fine, D. Lieb, and F. Rufeh, J. Chromatogr. 107, 351-357, 1975.

15. G. Herzberg, Molecular Spectra and Molecular Structure: Vol. II Infrared and Raman Spectra of Polyatomic Molecules, (D. Van Nostrand Company, Inc., New York, 1945).

16. J. R. Dyer, Applications of Absorption Spectroscopy of Organic Compounds (Prentice Hall, Englewood Cliffs, N.J. 1965).

17. Figure 2 was plotted using radiant flux data for an Apollo Model 550A CO_2 tunable infrared laser. See Laser Focus, 1978 Buyer's Guide 13th ed., p. 165.

18. (a) E. D. Hindley, Ed., Topics in Appl. Physics: Vol. 14 - Laser Monitoring of the Atmosphere (Springer-Verlag, Berlin, Germany, 1976).

(b) L. B. Kreuzer, Anal. Chem. 46, 239A (1974).

19. L. B. Kreuzer, J. Appl. Phys. 42, 2934 (1971).

20. J. R. Durig, S. F. Bash, and E. E. Mercer, J. Chem. Phys. 44, 4238 (1966).

21. J. R. Durig, W. C. Harris, and D. W. Wertz, J. Chem. Phys. 50 1449 (1969).

22. J. R. Durig and W. C. Harris, J. Chem. Phys. 51, 4457 (1969).

23. The Sadtler Standard Spectra, Gases and Vapors, Vol. 1, Spectrum Numbers GS106, GS107, and GS38 (Sadtler Research Laboratories, Inc., Philadelphia, Pa., 1972).

24. R. J. Brewer and C. W. Bruce, Appl. Opt. 17, 3746 (1978).

25. R. A. Crane, RCA Final Report EXC 93 (1976).

26. R. R. Patty, G. C. Russwurm, W. A. McClenny, and D. R. Morgan, Appl. Opt. 13, 2850 (1974).

27. A. Mayer, J. Comera, H. Carpentier and C. Jaussaud, Appl. Opt. 17, 391 (1978).

28. R. A. Crane, Appl. Opt. 17, 2097 (1978).

29. C. W. Bruce, and R. G. Pinnick, Appl. Opt. 16, 1762 (1977).

30. T. F. Deaton, D. A. Depatie and T. W. Walker, Appl. Phys. Lett. 26, 300 (1975).

31. C. W. Bruce, B. Z. Sojka, B. G. Hurd, W. R. Watkins, K. O. White, and Z. Derzko, Appl. Opt. 15, 2970 (1976).

32. C. W. Bruce, J. Opt. Soc. Am. 65, 1163A (1975).

33. C. K. N. Patel and R. J. Kerl, Appl. Phys. Lett. 30, 578 (1977).

34. J. I. Steinfeld et al., NASA-CR-148481, N76-28820 (1976).

35. See Ref. 19a: S. H. Melfi, Chapter 2 and R. T. H. Collis, and P. B. Russell, Chapter 4.

36. R. A. Weagant, and C. H. Beebe, Final Report, Contract Number J-LEAA-025-73 Laser Optoacoustic Explosives Detection, Beckman Instruments, Inc. (November 1977).

37. B. D. Green and J. I. Steinfeld, Environ. Sci. and Techol. 10, 1134 (1976).

38. J. A. Kerr, J. G. Calvert, and K. L. Demerjian, Chem. Br. 8, 252 (1972).

39. H. B. Singh, et al., J. Air Pollut. Control Assoc. 27, 332 (1977).

40. D. R. Cronn, et al., J. Geophys. Res. 82, 5935 (1977).

41. U.S. Dept. of Health, Education, and Welfare, Air Quality Criteria for Sulfur Oxides, National Air Pollution Control Administration Publication No. AP-50 (1969).

42. B. Seifert and D. Ullrich, Proceedings of the 13th International Colloquium, Studies in Environmental Science, Vol. I, Atmospheric Pollution (Elsevier Science Publishing Co., Amsterdam, 1978).

43. Low-resolution (2 cm^{-1}) spectral data taken from Ref. 23 as follows: toluene (GS 29), p-xylene (GS 31), chloroform (GS 72), and carbon tetrachloride (GS 73).

44. M. V. Zeller, Infrared Spectra of Nitrogen Oxides, Perkin-Elmer Infrared Bulletin IRB-48 (1974).

45. Stoker and S. L. Seager, Environmental Chemistry: Air and Water Pollution, (Scott, Foreman and Co., Glenview, Illinois, 1972).

46. U.S. Dept. of Health, Education, and Welfare, 1970. Air Quality Criteria for Hydrocarbons, National Air Pollution Control Administration Publication No. AP-64.

47. Selected Infrared Spectral Data, V. IX, Sec. B., American Petroleum Institute Research Project 44, Thermodynamics Research Center, Texas Engineering Experiment Station Texas A and M University, College Station, Texas, 31 October 1977.

48. Selected Infrared Spectral Data, V. I, American Petroleum Institute Research Project 44, Thermodynamics Research Center, Texas Engineering Experiment Station Texas A and M University, College Station, Texas, 31 October 1977.

49. (a) C. T. Pate, "Characterization of Vapors Emanating from Explosives," Analytical Research Laboratories, Inc., Monrovia, California (June 1976).

(b) J. Gelbwachs, Optics in Security: Law Enforcement 108, 10 (1977).

50. C. Pouchert, The Aldrich Library of Infrared Spectra, 2nd ed., (Aldrich Chemical Company, Inc., Milwaukee, Wisconsin, 1975).

51. A. Goldman, T. G. Kyle, and F. S. Bonomo, "Statistical Band Model Parameters and Integrated Intensities for the 5.9 μm, 7.5 μm, and 11.3 μm Bands of HNO_2 Vapor," Contract: F19628-68-C-0233, Project No. 8662, Scientific Report No. 7, Advanced Research Projects Agency, AFCRL-70-0091, January 1970.

52. E. C. Tuazon, A. M. Winer, R. A. Graham, J. P. Schmid, and J. N. Pitts, Jr., Environ. Sci. and Techol. 12, 954 (1978).

ABBREVIATIONS

ACGIH	American Conference of Governmental Industrial Hygienists
CO_2	carbon dioxide
DMA	dimethylamine
EPA	Environmental Protection Agency
FDH	formaldehyde dimethylhydrazone
FMH	formaldehyde monomethylhydrazone
MMH	monomethylhydrazine
NDMA	N-nitrosodimethylamine
NH_3	ammonia
NIOSH	National Institute of Occupational Safety and Health
O_3	ozone
OSHA	Occupational Safety and Health Administration
ppb	parts per billion
ppm	parts per million
SD	Space Division
SO_2	sulfur dioxide
TMA	trimethylamine
UDMH	unsymmetrical dimethylhydrazine

LABORATORY OPERATIONS

The Laboratory Operations of The Aerospace Corporation is conducting experimental and theoretical investigations necessary for the evaluation and application of scientific advances to new military concepts and systems. Versatility and flexibility have been developed to a high degree by the laboratory personnel in dealing with the many problems encountered in the nation's rapidly developing space and missile systems. Expertise in the latest scientific developments is vital to the accomplishment of tasks related to these problems. The laboratories that contribute to this research are:

Aerophysics Laboratory: Launch and reentry aerodynamics, heat transfer, reentry physics, chemical kinetics, structural mechanics, flight dynamics, atmospheric pollution, and high-power gas lasers.

Chemistry and Physics Laboratory: Atmospheric reactions and atmospheric optics, chemical reactions in polluted atmospheres, chemical reactions of excited species in rocket plumes, chemical thermodynamics, plasma and laser-induced reactions, laser chemistry, propulsion chemistry, space vacuum and radiation effects on materials, lubrication and surface phenomena, photosensitive materials and sensors, high precision laser ranging, and the application of physics and chemistry to problems of law enforcement and biomedicine.

Electronics Research Laboratory: Electromagnetic theory, devices, and propagation phenomena, including plasma electromagnetics; quantum electronics, lasers, and electro-optics; communication sciences, applied electronics, semiconducting, superconducting, and crystal device physics, optical and acoustical imaging; atmospheric pollution; millimeter wave and far-infrared technology.

Materials Sciences Laboratory: Development of new materials; metal matrix composites and new forms of carbon; test and evaluation of graphite and ceramics in reentry; spacecraft materials and electronic components in nuclear weapons environment; application of fracture mechanics to stress corrosion and fatigue-induced fractures in structural metals.

Space Sciences Laboratory: Atmospheric and ionospheric physics, radiation from the atmosphere, density and composition of the atmosphere, aurorae and airglow; magnetospheric physics, cosmic rays, generation and propagation of plasma waves in the magnetosphere; solar physics, studies of solar magnetic fields; space astronomy, x-ray astronomy; the effects of nuclear explosions, magnetic storms, and solar activity on the earth's atmosphere, ionosphere, and magnetosphere; the effects of optical, electromagnetic, and particulate radiations in space on space systems.

THE AEROSPACE CORPORATION
El Segundo, California